

https://dspace.org/

Model tests on double-hull wave interference effects using a gravity dynometer

Dacing, Anthony Aaron

2015-01-15
http://hdl.handle.net/10539/16562

Downloaded from a DSpace repository. https://dspace.org/

MODEL TESTS ON DOUBLE-HULL WAVE INTERFERENCE EFFECTS USING A GRAVITY DYNAMOMETER

Anthony Aaron Dancig

A dissertation submitted to the Faculty of Engineering, University of the Witwatersrand, Johannesburg, in fulfilment of the requirements for the degree of Master of Science in Engineering

Cape Town, 1987

DECLARATION

I declare that this dissertation is my own, unaided work. It is being submitted for the Degree of Master of Science in Engineering in the University of the Witwatersrand, Johannesburg. It has not been submitted before for any degree or examination in any other University.

Anthony Dancy

29th day of December 1987

ABSTRACT

The effects of wave interference between the hulls of double hulled ships was investigated with the use of a model towing tank fitted with a gravity dynamometer type of model towing system. The towing tank and measurement equipment were designed and built as part of the project, and will serve as a future testing facility at the University of the Witwatersrand.

The project continues from an investigation done to compare the drag of a Busemann Biplane Catamaran with that of a conventionally shaped hull, and focuses on wave interference effects on the drag of a conventional double hull ship as a function of speed and hull separation.

The accuracy and characteristics of the test equipment were determined and the experimental results were compared to other calculated data. The results clearly showed the relationship between wave drag, speed and separation resulting from wave interference effects and the magnitude of those effects.

CONTENTS

		Page
DECLARATION		i
ABSTRACT		ii
CONTENTS		iii
LIST OF FIGURES		v
LIST OF TABLES		ix
LIST OF SYMBOLS		x
1	INTRODUCTION	1
2	THEORY	5
2.1	Ship-Model Theory	5
2.2	Wave Interference	13
2.3	Preliminary Error Analysis	19
3	EQUIPMENT AND APPARATUS	21
3.1	The Towing Tank	21
3.2	The Towing Carriage	24
3.3	The Gravity Dynamometer	26
3.3.1	Pulleys	29
3.3.2	Accelerating Mass Retardation System	36
3.3.3	The Towline and Model Attachment	38
3.3.4	Model Speed Monitor	40
3.3.5	Model Speed Timer	41
3.3.6	Camera Activator	41
3.4	The Model	41
3.4.1	Model Design Considerations	42
3.4.2	Model Construction	45

4	TESTS	47
4.1	System Setup and Characteristics	47
4.2	*Testing Method*	53
4.3	Preliminary Tests	56
4.4	Repeatability Tests	60
4.5	Final Tests	62
4.6	Results Processing	63
5	DISCUSSION AND CONCLUSIONS	65
5.1	Accuracy of Tests and Calculations	65
5.2	Effects of Wave Interference	72
5.3	General	87
5.4	Recommendations for further work	88
REFERENCES		90
APPENDIX A		92
APPENDIX B		96
APPENDIX C		100
APPENDIX D		103
APPENDIX E		109
APPENDIX F		117
APPENDIX G		123
APPENDIX H		127
APPENDIX I		132

LIST OF FIGURES

Figure		Page
2.1	Results of skin drag tests (Todd[4])	11
2.2	Wave crests of diverging and transverse wave systems for a straight course at constant speed (Stoker[5])	15
2.3	Schematic interpretation of wave interference	16
2.4	Resistance of a sphere moving parallel to a solid interface versus speed (Havelock[7])	18
3.1	The towing tank	22
3.2	Schematic view of the towing tank	23
3.3	Layout of the gravity dynamometer system	31
3.4	Side view of the large driving pulley	32
3.5	Front view of the large driving pulley	33
3.6	The return pulley	34
3.7	The driving pulley	34
3.8	Side view of the return pulley	35
3.9	Accelerating mass retardation system	37

3.10	View of the towline to model attachment	39
4.1	A half size reduction of the grid network used to calculate wetted surface	51
4.2	Close-up view of a hull	52
4.3	Wave profiles on the hulls	52
4.4	A typical speed trace	55
4.5	Total drag versus Froude number	58
4.6	Wave drag coefficient versus Froude number	59
5.1	Percentage increase in wetted surface area versus Froude number	68
5.2	Percentage error in resistance ratio due to wall proximity versus Froude number	71
5.3	Wave drag coefficient versus Froude number	73
5.4	Resistance ratio versus Froude number (S/L = 0,18, S/L = 0,26)	74
5.5	Resistance ratio versus Froude number (S/L = 0,31, S/L = 0,34, S/L = 0,36)	75
5.6	Resistance ratio versus Froude number (S/L = 0,38, S/L = 0,41, S/L = 0,43)	76

5.7	Resistance ratio versus Froude number (S/L = 0,58, S/L = 0,81)	77
5.8	Resistance ratio versus separation/length ratio (Fn = 0,300 to 0,310)	79
5.9	Resistance ratio versus separation/length ratio (Fn = 0,315 to 0,325)	80
5.10	Resistance ratio versus separation/length ratio (Fn = 0,330 to 0,340)	81
5.11	Resistance ratio versus separation/length ratio (Fn = 0,345 to 0,355)	82
5.12	Resistance ratio versus separation/length ratio (Fn = 0,360 to 0,370)	83
5.13	Predicted resistance ratio versus Froude number (Everest[3])	85
5.14	Predicted resistance ratio versus separation/length ratio (Everest[3])	86
B1	Schematic view of pulley system	97
D1	Falling mass driving pulley	104
E1	Calibration chart for the speed monitor	

F1	Hull segments	118
H1	Circle and coordinates defining the model surface	128
H2	Coordinates, in millimetres, of the hull midship section	131
I1	Approximate increase in resistance in shallow water of unlimited width, deduced from model tests (Comstock and Hancock[11])	133
I2	Maximum size of model for no measurable wall effect (Comstock and Hancock[11])	134
I3	Increase in model resistance due to too large a model (Comstock and Hancock[11])	135

LIST OF TABLES

Table		Page
F1	Simpson's Rule applied to the hull segments for the calculation of surface area	120
F2	Simpson's Rule applied to the hull segments for the calculation of volume	121
G1	Repeatability test results at infinite separation	124
G2	Errors	125
G3	Percentage errors	125

NOMENCLATURE

Symbol	Quantity	Dimensions
a	acceleration	m/s^2
a	area	m^2
Cf	frictional resistance coefficient	-
Ct	total resistance coefficient	-
Cw	wave resistance coefficient	-
D	hull displacement	kg
d	*diameter*	m
F	force	N
Fd,Fr	frictional drag	N
Fn	Froude number	-
g	gravitational acceleration	m/s^2
h	height, or depth	m
I	mass moment of inertia	$kg.m^2$
K,A,B,C	constants	-
L	length of hull	m
Mf	bearing frictional torque	N.m
m,ma,mr, mw,mb	mass	kg
P	pressure	N/m^2
Re	Reynolds number	-
Rf	frictional resistance	N
Rt	*total resistance*	N
RW	wave resistance	N
Rwin	wave resistance at infinite separation	N
RW/Rwin	resistance ratio	-
r	radius	m
S	surface area	m^2
S/L	separation/length ratio	-
Tf	frictional torque	N.m

t	temperature	$^{\circ}C$
μ	coefficient of friction	-
V	volume	m^3
v	velocity	m/s
x,y,z,s, b,i,j,p	distance, or length	m
α	angular acceleration	radians/s^2
ρ	fluid mass density	kg/m^3
ν	fluid kinematic viscosity	$m^2.s$
ω	angular velocity	radians/s
θ	angle	radians

1 INTRODUCTION

This is a report of an investigation into the effects (negative and positive) of wave interference between the hulls of double-hulled ships. The word, double-hulled, or catamaran, is used here to imply two displacement hulls running side by side. The principle involved is that each hull generates its own set of waves, or wave system, the shape of which is a function of the power required to move the hull through the water at a given speed. If the sources of the wave systems are sufficiently close to each other, their wave systems will interfere and change shape, the new shape determining a new power-speed relationship. This implies that by adjusting the spacing between the hulls of a double hulled ship running at a certain speed one can obtain either an increase or a decrease in the power required to drive the ship at that speed.

The investigation also included the designing, building and instrumenting of an appropriate towing basin within certain constraints of space and time in order to carry out the investigation on a scale conducive to obtaining a reasonable degree of accuracy.

In 1970, a project was undertaken at this University to investigate and compare the drag of a Busemann Biplane Catamaran with that of a hull of conventional shape (see Bunt and Wells[1]). This was done on a very small scale with limited equipment and the water depth was restricted in order to make use of the hydraulic analogy: the analogy between the two dimensional supersonic flow of a perfect gas and the propagation of surface waves in shallow water. This investigation showed that a reduction in drag occurred due to wave

interference between the hulls and was dependent on the shape and separation of the two hulls. Due to the very small scale under which the investigation took place, however, nothing of any certainty could be said about how the principles demonstrated would apply to a full-size hull.

The former project of setting up a working towing tank facility at this University was initiated to further the investigation of the effects of wave interference between double hulls, with a view to being able to use the results to predict the performance of a full-size ship, i.e. to estimate possible power benefits from achieving the optimum speed-separation relationship for a particular double hull.

The practical use of catamaran ships has mainly been limited to vessels requiring a large deck area and high stability, such as passenger and vehicle ferries, cargo carriers and drilling rigs.

There are, however, numerous disadvantages to double hull ships. The inter hull portion is of limited depth, and is hence relatively useless. Extra weight and cost due to the bridging structure as well as providing two additional sides to the vessel, are appreciable. Two engine rooms are required, as well as two screws, rudders and sets of steering gear.

The overall accuracy or usefulness of the results obtained here is subject to certain limitations which are due mainly to the scale (physical size) of the equipment used. Only a limited amount of space was available for the location of the towing tank, and it was this which determined the width and length of run of the tank. With these dimensions fixed, the model dimensions could then be determined in order to give

the largest possible model size without adverse effects due to blockage and wave reflections from the tank walls. A large model size reduces the possibility and effects of laminar flow and increases the magnitude of the variables to be measured. It also reduces the scale factor between it and the full size ship. Model size therefore affects the size and type of towing apparatus, a larger model requiring a greater accelerating and towing force.

Due to the abovementioned tank size limitations the model dimensions could not be kept within the limits recommended to prevent laminar flow, and so a trip-wire was fitted to both hulls in an attempt to reduce its effect. Laminar flow however, will only affect the scaling up of the results to a full size ship, and not the comparison of results obtained at different separations. (This assumes that the boundary layer flow conditions around each hull are not significantly affected by the changes in separation of the hulls and are only a function of the speed.)

A gravity dynamometer system, such as the one used, has a major limitation in that it cannot determine a drag-speed relationship where the drag is decreasing with increasing speed. This becomes significant at points on the drag-speed curve where beneficial wave interference causes a sharp drop in drag (with increase of speed); as a result, the full extent of the drop will not then be detected.

It was not within the scope of this project to investigate fully the theoretical basis of wave interference. The mathematical theory of wave interference between double hulls is fully covered by Eggers[2]. Theoretical results obtained by Everest[3] were used to compare against the results of

this project.

Chapter 2 contains a discussion of the basic theory of ship-model testing and briefly covers wave interference. A preliminary error analysis was done prior to the design and setup of the testing equipment. This is also detailed in Chapter 2. The equipment used for the project is described in Chapter 3, and Chapter 4 covers the setup and characteristics of the equipment, as well as the testing procedures which were used. The results were all presented graphically and are discussed in Chapter 5.

2 THEORY

2.1 Ship-Model Theory

The resistance of a model or ship is usually measured by the force which would be necessary to tow her through smooth water, and the power so expended is called the tow-rope or effective power.

Four different components go to make up the total resistance of a model or ship:

(i) Skin friction resistance, due to the movement of the hull through a viscous fluid. A layer of water surrounding the hull is given a forward velocity and after the ship has passed, this remains as a frictional wake. The momentum in this wake comes from the ship, and during the ship's passage is a continuous drain of energy and hence a source of resistance. It amounts to as much as 80 per cent in total in slow cargo ships and still some 50 per cent in the case of high-speed warships.

(ii) Wave making resistance. A body moving in a fluid creates a pressure field around it, which in the presence of a free surface results in the formation of a wave system. The constant formation of the wave system results in further energy drain.

(iii) Eddy resistance, due to the energy carried away by eddies formed around stern fittings, plate overlaps, or local regions where the hull curvature is so sharp that the water breaks

away. This last kind of eddy r istance is sometimes referred to as separation resistance, since it is accompanied by a separation of the boundary layer from the hull surface.

(iv) Air resistance is caused by the movement of the above-water part of the hull through the air. In average cases this amounts to only some 2 per cent of the total. This is not significant in model tests and must be allowed for separately.

The above division of the total resistance is convenient but not strictly scientifically correct, since the first three types all react with one another. For example, the skin drag gives rise to a boundary layer which effectively alters the shape of the hull and hence the pressure distribution and the resulting wave-making resistance, while the wave system in turn alters the wetted surface area and so the skin friction resistance. Nevertheless it is convenient to make such a division for practical purposes.

Assuming that the resistance of a model moving on the surface of a real fluid depends upon certain properties of the fluid, the size of the model, and the speed at which the model is moving, dimensional analysis may be used to find the form of the parameters which must be held constant in any change of scale in order that the flow patterns may be geometrically similar.

Let:

R_t = total resistance of the hull

ρ = mass density of the fluid

v = velocity of the hull

L = length of the hull

ν = kinematic viscosity of the fluid

g = gravitational acceleration

P = pressure per unit area at any point in the fluid

S = wetted surface area

If Rt is assumed to be a function of these quantities and the theory of dimensions is applied, we find that,

$$Rt/\rho v^2L^2 = f[vL/\nu, v^2/gL, P/\rho v^2] \qquad (2.1)$$

Since the wetted surface S of similar forms is proportional to L^2, we can write the left-hand side of the equation in the more usual form of a specific total resistance coefficient Ct;

$$Ct = 2Rt/\rho Sv^2$$

$$= f[vL/\nu, v^2/gL, P/\rho v^2] \qquad (2.2)$$

Dimensional analysis does not give any further assistance in determining the form of the function f. The equation states in effect that if all the parameters on the right-hand side have the same values for two geometrically similar but differently sized bodies, then the flow patterns will be similar and Ct will be the same for each.

Considering firstly the case of a non-viscous fluid, so that there is no skin drag, and neglecting the last term $P/\rho v^2$, we have left the wave making or residuary

resistance, which for similar forms is a function of the hull size L, the velocity v and the gravitational acceleration g. Hence we can write the wave-making resistance coefficient as

$$C_W = 2R_W/\rho S v^2$$

$$= f_1[v^2/gL] \qquad (2.3)$$

This means that geometrically similar bodies of different size will have the same wave-making resistance coefficient Cw if they are run at the same value of the parameter v^2/gL.

William Froude early recognized the necessity of dividing the resistance up into separate components. Based on the general law of mechanical similarity and from experiments on models of the same shape but different dimensions, and on observation of their wave patterns, Froude stated in his Law of Comparison that:

"The resistance of geometrically similar ships is in the ratio of the cube of their linear dimensions if their speeds are in the ratio of the square roots of their linear dimensions."

Defining the Froude number as

$$Fn = v/\sqrt{(gL)}$$

the above implies that for the same value of Fn for model and ship,

$$R_{W_S}/D_S = R_{W_m}/D_m$$

where we define:

Rw = wave resistance

D = hull displacement

s,m = subscripts representing ship and model respectively

At the same Cw, the corresponding speed for the model is always far less than that of the full-size ship, thus allowing models to be run at easily obtainable speeds in a towing tank.

Returning to equation (2.2) and the term $P/\rho v^2$, neglecting atmospheric pressure, and referring P only to the water head, then for corresponding points in the model and ship P will vary with the linear scale ratio. At corresponding speeds v^2 also varies in the same way, so that $P/\rho v^2$ will be the same for model and ship provided that they are run in the same fluid. In practice, atmospheric pressure remains the same for model and ship, making the value of $P/\rho v^2$ at corresponding points much larger for the model than for the ship. The hydrodynamic forces which we are concerned with in model tests arise from pressure differences, so that the parameter $P/\rho v^2$ will be taken care of at corresponding speeds as long as the fluid remains in contact with the model and ship surfaces. When flow separation occurs, the similarity requirements will no longer be fulfilled.

The first term of equation (2.2) involves the fluid viscosity and we can write the frictional resistance coefficient as

$$Cf = 2Rf/\rho Sv^2$$

$$= f_2[vL/\nu]$$

The value of Cf will be the same for model and ship providing that the parameter VL/ν is the same. If both ship and model are run in water at about the same temperature, so that ν has the same value, this becomes:

$$V_s L_s = V_m L_m$$

This condition is very different from that of the wave-making resistance, in that as the model size decreases, the speed of test must increase.

It is obvious that both conditions of similarity cannot be satisfied in a single test unless the model is towed in a fluid with a kinematic viscosity far less than that of water. The only practical way of overcoming this is to separate the wave-making and frictional resistances. Hence we write:

$$Ct = CW+Cf$$

The frictional resistance is calculated by comparing the hull suface to that of a smooth flat plank. Numerous skin friction formulations have been developed through drag tests on flat planks which relate the frictional resistance coefficient Cf to the parameter VL/ν, commonly known as the Reynolds number,

$$Re = VL/\nu$$

Figure 2.1 shows the results of various independent tests on smooth planks. The chart shows that at Reynolds numbers below about $5x10^6$, many of the results fall below the general level as speed is decreased. This is due to the fact that at low speeds much of the surface is in a region of laminar flow.

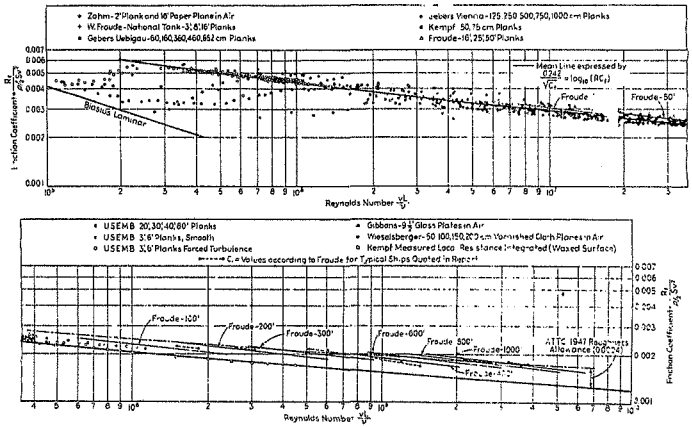

Figure 2.1 Results of skin drag tests
(Todd(4))

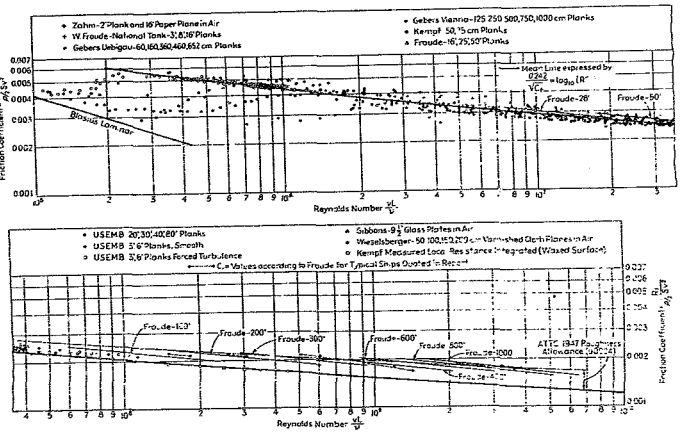

Figure 2.1 Results of skin drag tests
(Todd(4))

For complete laminar flow, the values of Cf for a smooth plank have been calculated by Blasius to lie on the lower line.

As speed is increased for a plank of given length, turbulent flow gradually spreads forward and as the resistance in tubulent flow varies as a higher power of v than laminar flow, the resistance curve rises toward an upper limit.

By artificially stimulating turbulence by using a trip wire or a strut ahead of the plank, even small planks at low speed can be run in the fully turbulent condition.

Cf values falling between the upper and lower curves are said to be those for transitional flow. In practice, unless turbulence is artificially stimulated, there will be some zone of laminar flow at the leading edge of all the planks. However, as the length of plank and speed are increased, giving higher Reynolds numbers, the area in laminar flow grows smaller and its proportional effect on resistance decreases.

Schoenherr made a statistical survey of most of the available experimental data, and drew the mean line shown on the chart. The formula for this line is:

$$0{,}242/\sqrt{(Cf)} = \log(ReCf)$$

The friction line used for this poject was the Prandtl-Schlichting line for all turbulent flow, as Cf is then more easy to compute.

$$Cf = 0{,}455/(\log Re)^{2{,}58}$$

2.2 Wave Interference

It is an experimentally established fact that the wave resistance of a ship increases rapidly with speed, but the increase does not follow a simple power law, i.e. one such that the resistance is proportional to a positive power of the speed. The resistance-speed curve in fact exhibits considerable "waviness" which is due to interference between some of the waves in the overall wave system poduced by the hull.

This can be explained in a general way if it is assumed that the resultant wave system of the ship is mainly due to two sources of disturbance, one situated near the bow and the other near the stern, these being the regions where the cross-sectional area of the hull changes rapidly; the approximately parallel middle part of the ship is relatively ineffective in generating waves. If the speed of the ship is such that the wave trains generated at the bow and stern reinforce each other, a large amount of energy will be expended in the waves and the resistance will be high. However, if the two wave systems largely annul each other by interference, the resistance will be low. This explains the waviness in the curve of resistance on a base of speed.

The overall wave system surrounding a moving hull consists basically of two components: a diverging wave system and a transverse wave system. The two systems move roughly at right angles to each other, with the transverse wave crests at right angles to the direction of motion of the hull. A diagrammatic representation of the wave crests of the diverging and transverse

systems is shown in Figure 2.2.

It can be seen that the wave system is confined to a fixed area which is defined by straight lines at an angle of arcsin(1/3) (about 20 degrees) to the ship's course. This angle remains constant irrespective of the speed of the hull as long as the latter is constant. The magnitude of the waves outside the defined area is not zero, but is of a much smaller order than the waves inside.

In a double hull arrangement, the inside diverging wave systems of each hull may meet each other on the centre plane between the two hulls, and are then reflected. Thus, instead of these waves travelling across toward the stern of the opposite hull, they are reflected on the centre plane and travel back toward the stern of the same hull whose bow generated them (see Figure 2.3).

Theoretically, then, the separation within which interference will take place should be the waterline length multiplied by the tangent of 20 degrees. As the separation increases from this value, the reflected bow waves will begin to pass behind the stern and so have less and less effect on the overall wave system of the hull.

The resulting wave interactions are far more complex than those described above. Eggers[2] gives equations for the calculation of the wave resistance for a double hulled ship, based on the work done by Michell[6].

Havelock[7] also developed a method for calculating the mutual interactions between two bodies moving in a fluid. The method applies for bodies lying in any position relative to one another. For the case where

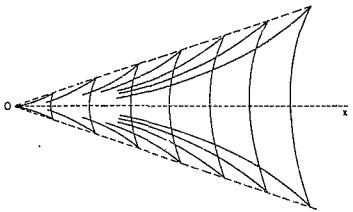

Figure 2.2 Wave crests of diverging and transverse wave systems for a straight course at constant speed (Stoker[5])

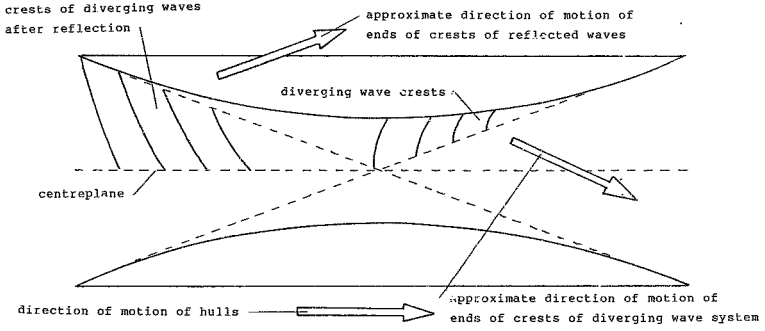

Figure 2.3 Schematic interpretation of wave interference

the two bodies are moving parallel to one another, Havelock tabulates the results for two spheres in terms of the dimensionless resistance of one sphere and a dimensionless speed. Each curve in Figure 2.4 represents a different separation between the two spheres.

Here,

R = the wave resistance of a sphere in the direction of motion

c = the velocity of the sphere

b = the radius of a sphere

2k = the distance between the centres of the spheres

f = the depth of a sphere from the free surface

These results can be interpreted as being for a single sphere moving parallel to a solid interface. The results show that wave resistance increases with increasing nearness to the interface.

Havelock[7] also shows that with the spheres in any relative position, effects of wave interference occur when the following sphere lies within the wave pattern produced by the leading sphere, and arise from both the transverse waves and the diverging waves.

Everest[3] expanded on the theoretical work done by Eggers and used measured wave making properties of the individual hulls to predict the performance of the double hull configuration, thus eliminating the mathematical difficulties and approximations of

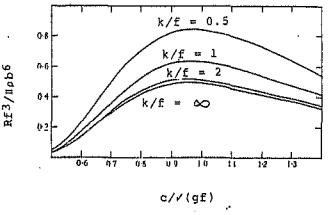

Figure 2.4 Resistance of a sphere moving paralell to a solid interface versus speed (Havelock(7))

accurately representing a practical hull shape.

2.3 Preliminary Error Analysis

A preliminary error analysis was done in order to determine the effect which the different variables have on the overall results. This was essential for the proper design and choice of the measuring system and instrumentation as well as the design of the model (see Appendix A).

The analysis indicated the importance of designing a hull which would have a large wave-making or residuary resistance as compared to the frictional resistance.

For the determination of the effects of wave interference between the hulls, the quantities which must be examined are the total drag of the model as a function of speed and separation and more importantly the wave drag coefficient or the wave drag as a function of speed and separation.

Total drag of the model is measured directly by the gravity dynamometer (less friction), and so is not influenced by any other measured or calculated variables. The wave drag and wave drag coeficient are however arrived at through the measurement of the following variables;

- model velocity
- total model drag
- total wetted surface area of the moving model
- temperature of the tank water

The results of different tests were used in the calculations. These were found in the literature (see Appendix A).

3 EQUIPMENT AND APPARATUS

3.1 The Towing Tank

An area of 16 m by 3 m was allocated for the siting of the towing basin, giving a maximum possible length of run of 15 m.

The tank was constructed from Braithwaite plates and so had to be supported above the ground in order to bolt the bottom plates together. For this, U-shaped frames were constructed from 127 mm by 76 mm steel I-beam. The vertical sides of the frames provided support for the tank walls (normally internally supported by cross-beams). The frames were attached to the wall plates by means of two slotted brackets so as to allow easy alignment of the wall plates. The exact tank dimensions were, 15,9 m long by 2,44 m wide by 1,22 m deep (see Figures 3.1 and 3.2).

An outlet pipe was placed at a height of 1 m from the tank bottom and this set the water-level. When not in use, the water was circulated through the underground sump of the Mechanical Engineering Laboratory, a procedure which kept the water surface free from deposits.

A 1 m wide walkway was constructed along one side of the tank to facilitate easy access to the water surface and the towing trolley system.

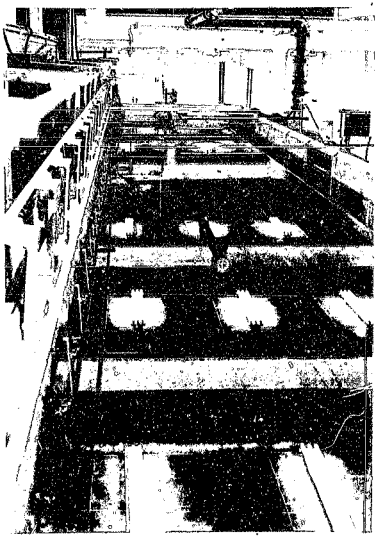

Figure 3.1 The towing tank

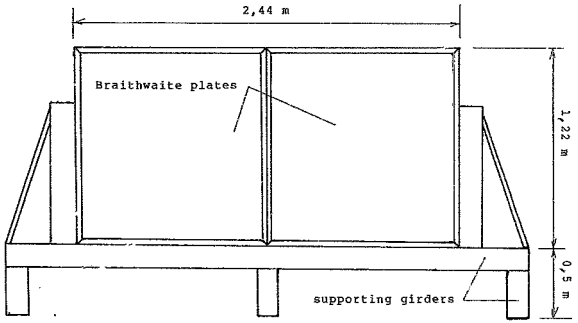

Figure 3.2 Schematic view of the towing tank
(end view)

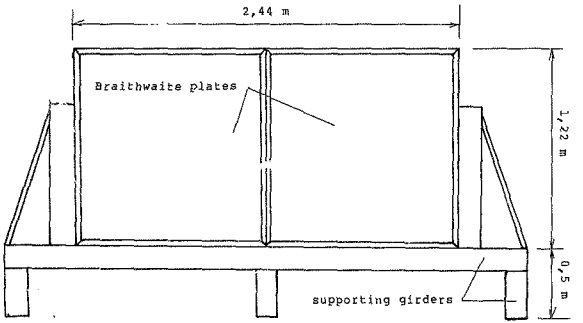

Figure 3.2 Schematic view of the towing tank (end view)

3.2 The Towing Carriage

A commercial ship-model towing trolley system was obtained for installation on one side of the tank. (Although designed for the demonstration of basic principles in Naval Architecture, it was later found that the apparatus needed to be considerably upgraded to produce sufficiently accurate results.)

The towing trolley ran on two cylindrical stainless steel rails, one mounted on the top of the tank wall and one against the inner surface of the wall. Two pairs of wheels arranged with their axes located at right angles bore on the top rail and a further wheel bore against the lower rail. The wheel rims were coated with hard rubber and one wheel was driven by a variable speed low voltage direct current motor through a reduction gearbox.

The trolley was controlled through a control panel carrying isolating and reversing switches, a speed regulator and an electrically controlled stop clock for measuring trolley speed. Current was fed to the trolley by means of a trailing cable.

Contacts at each end of the track brought the trolley automatically to rest at the end of its run, and two contacts located a measured distance apart actuated the stop clock for speed measurement.

A tubular beam, attached to the trolley and projecting into the tank, carried the model support and force dynamometer. This comprised a pivoted lever carrying

at its lower end a transverse rod, the end of which engaged the model. A second lever was attached by way of a flexible cable to a spring balance fitted with a dashpot. A pointer moving over a curved scale indicated the traction force. This reading was taken visually while the trolley was in motion.

Preliminary tests using a 1,2 m R.I.N.A. standard tanker model which was supplied with the trolley apparatus indicated that the force dynamometer would be inadequate for the accuracy which was required and so an electro-mechanical force transducer was designed and installed.

The force transducer consisted of a cantilevered beam fitted with strain gauges. This was attached to the tubular beam projecting from the trolley. The free end of the cantilever was attached to the model, the drag force then being picked up by the strain gauges as a bending moment in the beam. A configuration of four active strain gauges was used to compensate for torsion and temperature effects. The length of the cantilever was adjustible so as to provide the largest possible output signal for the range of drag being measured. Output and input signals from the force transducer were carried along with the trailing cable, the output being fed into a chart recorder.

A basic operating error proved to be the fact that electrical interference from the trolley motor produced an offset error proportional to the speed setting of the trolley as well as a sine wave in the actual output. The installation of shielded cabling on all wiring annulled the offset error and a filter was designed to average out the sine signal. This produced a clean signal when the trolley was run without load.

When the trolley was loaded, an unstable output signal was produced and a quantitative value for drag could not be determined with any reasonable accuracy. The instability was put down to the following effects:

- lack of stiffness in the tank walls, rail supports, rails and transducer support beam;
- out of roundness of trolley wheels; and
- pitching of the model due to sudden acceleration whenever the trolley motor was activated.

3.3 The Gravity Dynamometer

In order to be able to obtain an acceptable drag reading, a major re-design of the trolley system would have had to be undertaken. Due to the time factor involved, the trolley system was therefore scrapped and a special gravity dynamometer designed, built and installed.

The advantages of a gravity dynamometer over a trolley system are:

- a much smaller amount of hardware and instrumentation is required for the same accuracy;
- ease of setup and alignment;
- there are no stiffness problems to be overcome; and

. hardware and instrumentation are relatively simple and quick to construct.

Its disadvantages are:

. model shapes which develop a side force, e.g. single asymmetrical models, cannot be tested;

. speeds at which the resistance is decreasing with increasing speed cannot be used;

. friction in the system must be determined and allowed for; and

. more runs are required per test point.

A gravity dynamometer type of towing system implies that the model towing force is applied by a falling mass, giving a steady, constant and accurately determinable drag force. This is normally done using a system of pulleys. Depending on the length of run available and the size of the model, an additional accelerating mass is sometimes required in order to bring the model up to the correct speed in as short a distance as possible. The accelerating mass is then removed from the system, the model then being towed by the drag mass only. With the towing force fixed, the model speed is then determined.

A mathematical analysis was performed on a basic gravity dynamometer system. For this, it was assumed that the drag force would be proportional to the square of the model speed, and that an accelerating mass would be required in order to bring the model up to the correct speed within a certain distance (see Appendix

B).

Analysis of the characteristics of the system showed the following:

- without an accelerating mass the model speed will only asymptote to the correct drag-speed relationship;
- as the applied drag mass increases, the error in speed decreases;
- an accelerating mass will bring the model speed closer to the correct speed in a shorter distance and hence reduce the speed error; and
- an over-acceleration will cause an instability in the system since the speed will only satisfactorily asymptote as the drag is increasing.

Formulae were derived to calculate the required accelerating mass necessary to bring the model up to the correct speed within a given accelerating distance, as well as the percentage error in speed due to not using an accelerating mass (see Appendix B).

In the derivation of the formulae it was assumed that the model drag was proportional to the square of the model speed, whereas in practice the drag-speed relationship for a particular hull exhibits "humps and hollows" due to the shape of its wave system, and hence does not continuously follow this relationship. The formulae were however useful for design purposes and as a first approximation in calculating the required accelerating mass for a particular test point.

From the analysis it was clear that it would be necessary to monitor the model speed continuously from rest in order to determine whether the model had reached its asymptotic value of speed and that it was travelling under steady flow conditions for the correct distance before its speed was measured, i.e. that the accelerating mass was correct (establishment of the flow requires constant speed for a distance of approximately eight model lengths, Shiells[8]).

The accelerating mass acts in conjunction with the driving mass from the start of the run and after a fixed distance it is lifted from the system. (It was found that the accelerating mass must be removed slowly since sudden removal of the mass from the system causes the model to undergo pitching oscillations for the rest of its run.)

A method was devised to calculate the amount of friction present in the unloaded gravity system using the priciple of conservation of energy (see Appendix D).

3.3.1 Pulleys

The basic gravity dynamometer which was built and installed in the tank consisted of a continuous towing line running between pulleys at either end of the tank, and two separate driving lines which ran from one of the towing line pulleys over a separate set of pulleys mounted on the ceiling above the tank. (The towline pulley onto which the driving lines were attached will be referred to as the driving pulley, the pulley at the opposite side of the tank being the return pulley.)

Figure 3.3 shows the overall layout of the gravity dynamometer system, while Figures 3.4 and 3.5 detail the large driving pulley. Figures 3.6 and 3.7 are photographs of the return and driving pulleys respectively.

The return pulley was mounted on a pivoting pole so as to allow free movement in a vertical plane along the direction of travel of the model, the pulley being held in this plane by a tensioning mass which kept the towline under a fixed tension and compensated for any stretch in the towline. The return pulley is detailed in Figure 3.8.

An adjusting screw on the pivot pole facilitated levelling of the towing line with the water surface. The pulley was held in a slotted bracket, which in turn was bolted onto the pivot pole by a single bolt, allowing easy pulley alignment in all directions. The pulley wheel was machined from aluminium with a V-slot to take the tow line. A small self-aligning ball bearing was press fitted into either side of the pulley and a mild steel shaft passed through the bearings and located in the slotted bracket.

Figure 3.3 Layout of the gravity dynamometer system

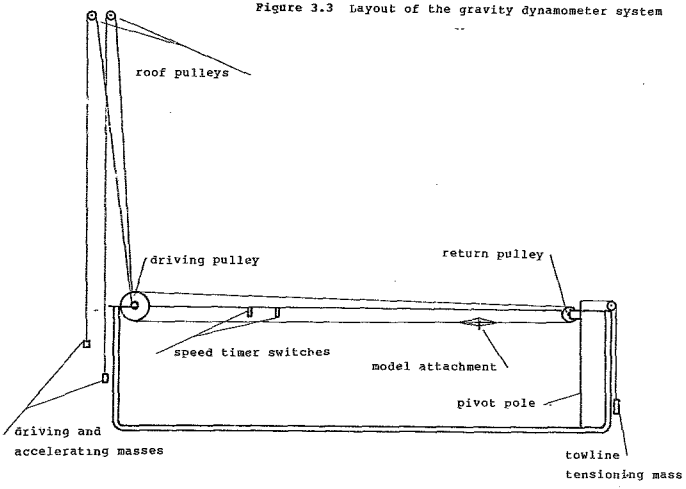

Figure 3.3 Layout of the gravity dynamometer system

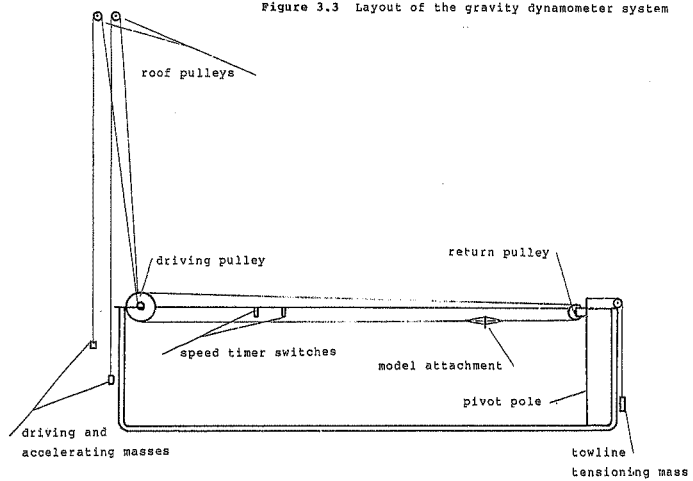

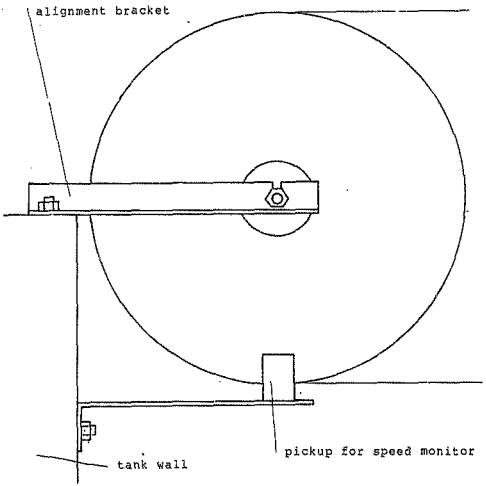

Figure 3.4 Side view of the large driving pulley

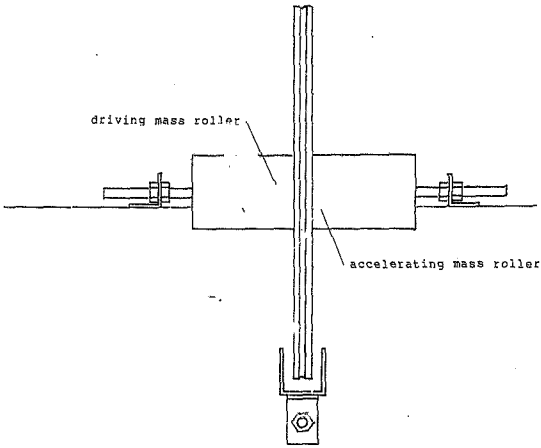

Figure 3.5 Front view of the large driving pulley

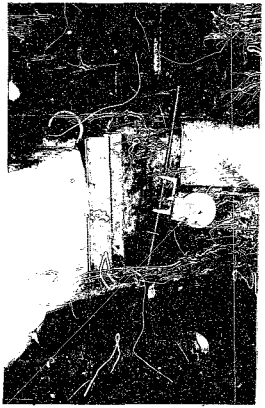

Figure 3.6 The return pulley

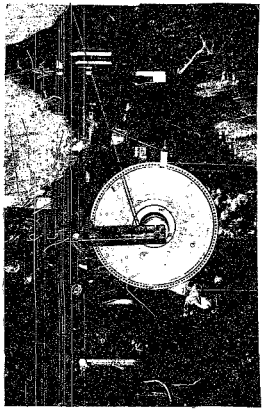

Figure 3.7 The driving pulley

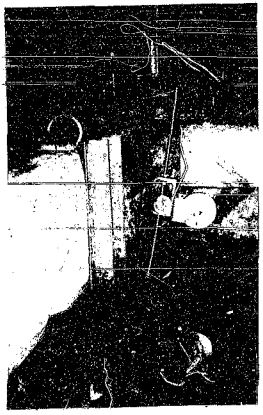

Figure 3.6 The return pulley

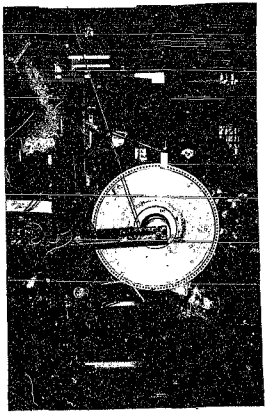

Figure 3.7 The driving pulley

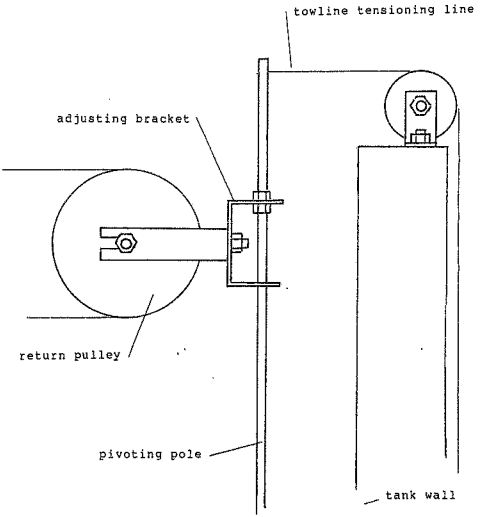

Figure 3.8 Side view of the return pulley

The driving pulley was made up of one large 253 mm diameter aluminium pulley attached to two smaller, 51 mm diameter hollow steel rollers which lay on either side of it: one side for the driving line and the other for the accelerating line. The driving and accelerating lines were wound up onto the rollers. The driving pulley ran on bearings in the same way as the return pulley and was fastened to the tank wall by a slotted bracket, so allowing for alignment and height adjustment.

From the driving pulley rollers, the accelerating and driving lines passed over small pulleys mounted on the ceiling. This gave a 3,2 m drop from ceiling to floor. With a 5:1 diameter ratio between the large pulley and the rollers, a length of run of 15 m was obtained.

3.3.2 Accelerating Mass Retardation System

The accelerating line passed through a retarding spring which caught onto the line after it had moved a fixed distance. The spring gently reduced the effect of the mass on the system until the moment when it supported the mass completely. A separate mass was hung from the spring to pre-stretch it and so help reduce the suddenness of application of the retardation force.

The accelerating line was attached to the roller by means of a small hook which then detatched once the accelerating mass was fully supported by the retarding spring (see Figure 3.9).

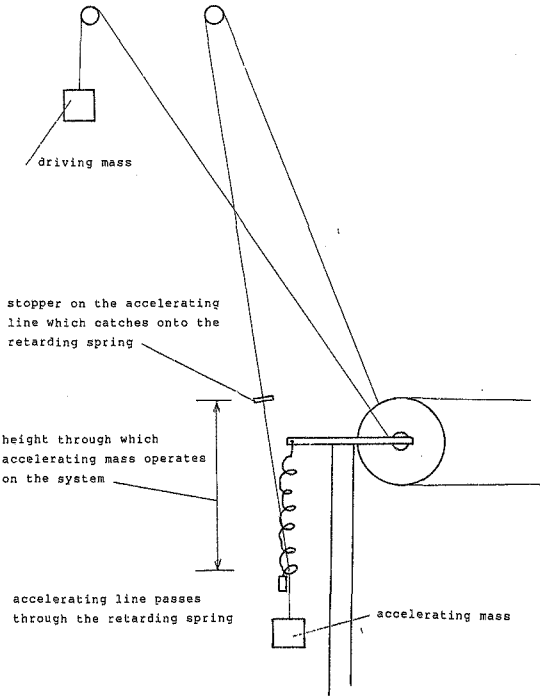

Figure 3.9 Accelerating mass retardation system

3.3.3 The Towline and Model Attachment

A towline is required to be strong, light, of low stretch and have a small diameter to keep the friction in the system down to a minimum. A 1,0 mm diameter woven nylon thread was used for this purpose.

The force in the towline was transferred to the model by way of a vertical aluminium pin against which the model bore, allowing the model free up and down movement due to sinkage and changes in trim, as well as facilitating easy attachment of the model to the towline. The pin was held rigidly to the towline by means of a light piano wire brace. Holes were drilled through the pin to reduce its weight (see Figure 3.10).

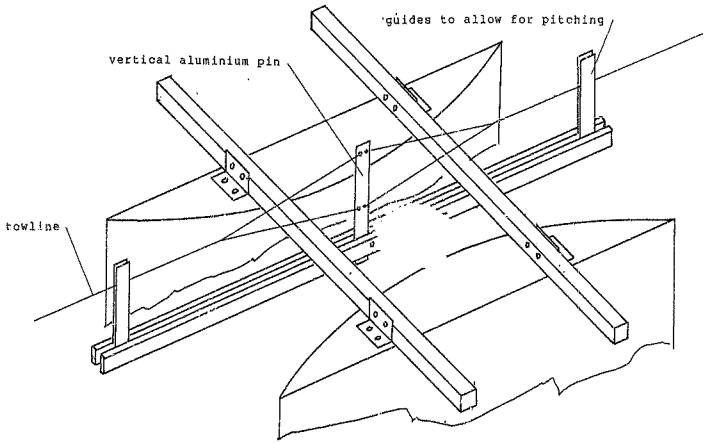

Figure 3.10 View of the towline to model attachment

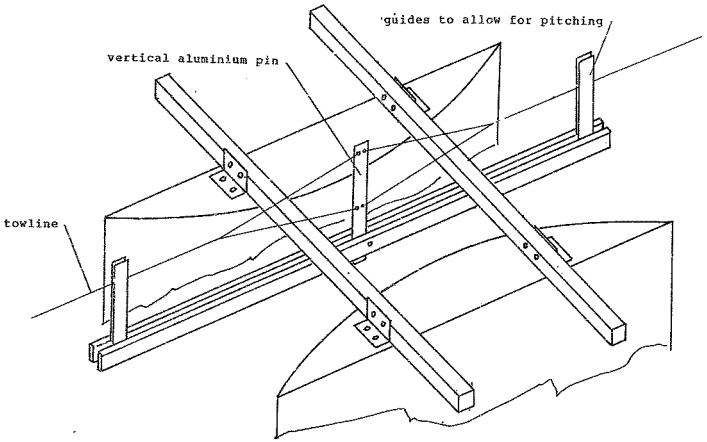

Figure 3.10 View of the towline to model attachment

3.3.4 Model Speed Monitor

Since the model speed is directly proportional to the speed of the driving wheel, the model speed could be monitored by using electrical pulses which were generated by the rotation of the driving wheel, the frequency of the pulses being directly proportional to the model speed.

The pulses were generated by a photo-transistor and l.e.d. combination, with the driving pulley in between the two devices. Equally spaced holes drilled through the driving pulley on the largest possible diameter produced the pulses. The pulses from the photo-transistor were fed into a standard frequency to voltage converter micro-chip, then to a zero setting device and then into a chart recorder.

The spacing, diameter and number of holes required were determined by the range of speed which the device was required to measure, as the photo-transistor has a set turn-on/off time and the frequency to voltage converter a set frequency operating range. The device was designed to monitor or measure model speeds from 0,0 to 2,0 m/s, which for a model length of 1,2 m (4 ft), gave a maximum Froude number of 0,58.

The signal in the chart recorder could be amplified to indicate a change in speed of 0,004 2 m/s per chart division, which for a model speed of 1,0 m/s indicates a change in model speed of 0,4 per cent per chart division (see Appendix E).

3.3.5 Model Speed Timer

Actual model speed at the end of the run was determined by timing the model over a known distance using a standard timer-counter instrument. The on and off pulses which activated the timer were transmitted when the aluminium pin on the towline passed between two sets of photo-transistor and l.e.d. switches spaced 1,0 m apart, the pulse being transmitted when the light beam was broken.

3.3.6 Camera Activator

For the purposes of recording the wave profile along the hull and for calculating the wetted surface area a photograph was taken of the moving model as it passed through the first speed timer switch. The pulse from the switch activated a relay which in turn released a spring loaded solenoid. The solenoid was mounted above the shutter release button of a standard S.L.R. camera, and when the current in the solenoid was turned off, the spring in the solenoid pushed the central rod onto the shutter release button.

3.4 The Model

It was first intended to test diamond-shaped as well as parabolic-shaped hulls as done by Bunt and Wells[1]. However it was obvious that a hull shape with a large discontinuity on the waterlines, such as a diamond shape, would not offer any hydrodynamic

advantages over a practical hull shape.

Because wave interference will occur between any two hulls running next to each other, irrespective of the shape of the hulls, the choice of shape is not influenced by whether interference will take place or not, but rather by the extent of the interference. The amount of interference is determined by the size of each hull's diverging wave system. For experimental purposes the extent of interference will determine what accuracy and resolution the readings must show in order to obtain meaningful results.

3.4.1 Model Design Considerations

The preliminary error analysis indicated the importance of having a hull shape which has a large residuary resistance as compared with frictional resistance. For this purpose the literature was consulted to determine what hull shape characteristics influenced the residuary resistance. It was found that in general, for most shapes at high Froude numbers, residuary resistance is mainly dependent on the displacement ratio. This is the ratio of the hull displacement to the hull length, Barnaby[9]. Thus for any hull of fixed length running at high Froude numbers, increasing the hull displacement will cause an increase in residuary resistance.

This implies that the model should be designed in such a way as to facilitate large adjustments in displacement, i.e. high freeboard, so as to ensure high residuary resistance without having to re-design and build another model to change the displacement ratio.

Changing the displacement of the hull by changing ballast means that the draft will change, but beam/draft ratios play a relatively minor part when compared with the displacement ratio at high Froude numbers (see Barnaby[9]).

Factors which have to be considered in the choice of a suitable hull shape for wave interference tests are;

- the shape must be easy and quick to construct in duplicate;
- the shape must produce a large enough diverging wave system;
- the shape must be close to that of a normal ship, i.e. hydrodynamically efficient; and
- the shape should be easily representable mathematically for possible wave interference calculations as well as for displacement and wetted surface area calculations.

The major factor which determines the model dimensions is the size of the tank in which the model is to be tested.

The cross-sectional areas of the model and of the tank are related in that due to the speed of the model a back flow is produced which increases the virtual speed of advance of the model; this is known as blockage. Birt[10] considers that the model cross-sectional area should not exceed 1 per cent of that of the tank.

Wall effect due to the model being in close proximity to the sides and bottom of the tank causes an increase

in the measured resistance of the model. Comstock[11] gives tables for determining the maximum length of of a model for no measurable wall effect based on model speed and displacement, as well as the expected increase in resistance due to an oversized model. Also, the expected increase in resistance due to shallow water effects is tabulated.

Wave reflections from the tank wall which do not pass clear astern of the model will affect the wave system around the hull and hence produce an error (see Barnaby[9]). The wave system for a hull moving at any speed through the water is confined to a fixed area around the hull and so for any model length, the hull to wall distance for no interference can be calculated.

Because the full size ship will always operate under turbulent flow conditions, it is important to ensure that the model does the same. Laminar flow will produce a large error if the model results are scaled up to full size, while transitional flow will affect the repeatability of the results. Birt[10] and Todd[4] give a minimum Reynolds number of 10×10^6 to ensure turbulent flow without artificial stimulation. The disadvantage of using a small towing basin and hence small models is that the Reynolds number seldom exceeds the above value and so artificial stimulation is normally necessary. A trip wire is normally used for this purpose and is placed at 5 per cent of the waterline length from the bow (see Todd[4] and Allan[12]).

From the above it is clear that in order to reduce any effects of laminar or transitional flow, the model should operate at as high a Reynolds number as possible, and hence should be as large as possible.

The above points were all taken into account to fix the overall model dimensions, as well as the gravity dynamometer speed range and the proposed Froude number range over which the model was to be tested.

In order to ensure that the model would perform within the bounds of normal ship types, i.e. perform as a typical ship, beam, draft and displacement-length ratios of various ships were determined and the model ratios chosen accordingly.

The model waterlines were designed as arcs of circles; any point on on its surface could thus be mathematically defined in terms of x, y and z components (see Appendix H).

Each hull was asymmetrical with one flat side and one curved side. This made manufacture easy as there were only two surfaces instead of four which had to be shaped (the hulls were hand shaped). There was also an advantage in that the flat sides generated a much smaller wave system than the curved sides, so allowing for a longer model without adverse effects due to wave reflections from the sides of the tank. To simulate a situation of infinite hull separation, the hulls were aligned with the flat sides facing inwards, which resulted in a negligible wave interference pattern between the hulls, while for all other tests the hulls were aligned with the curved sides facing inwards. The hulls were 800 mm long, with a beam of 8[illegible] mm.

3.4.2 Model Construction

The model was constructed from wooden sections, each

section being a "waterline" of 8,4 mm thickness. All waterline sections were glued together to make up the basic hull shape. Body filler was used to fill in the overlaps between the sections so as to give a smooth and fair shape. The first side of the hull provided a reference for alignment of the sections and for final shaping. Templates of each section were used to ensure that both hulls were as identical as possible. The hulls were coated with clear polyurethane paint applied with a spray gun to give a smooth, uniform and watertight finish.

A 1,5 mm diameter lead wire was attached around the hull to act as a turbulence stimulator.

The hulls were held together by an aluminium frame. Steel brackets attached to each hull, and bolted onto the frame, allowed easy adjustment of the spacing between the hulls as well as correct alignment. Two pairs of vertical aluminium struts along the centreline of the frame, one pair at the bow and the other at the stern, were located on either side of the towing line in order to keep the model in a straight line, since the towing force was applied at the longitudinal centre of gravity of the model (see Figure 3.10).

4 TESTS

4.1 System Setup and Characteristics

Initial tests were run in order to determine the optimum towline tension for the system. System friction increases with increasing towline tension, while too low a tension allows intermittent slippage between the towline and the driving wheel, giving an oscillating speed trace and hence an incorrect speed reading.

Slippage was checked by aligning a mark on the towline with a mark on the driving pulley. The model was driven at the maximum test speed after which the alignment of the marks was re-checked. Slight creep of the towline along the driving pulley due to stretch in the towline occurred at all towline tensions, but this only amounted to around 5 mm over a length of run of 12 m.

It was found that the direction of towing of the model had a large effect on the amount of towline tension required to prevent slipping. The tension required when the model was towed directly by the driving pulley was far less than that required if towed via the return pulley.

Once the towline tension was set the system friction was determined and recorded. Subsequent checks indicated that the system friction remained constant throughout the duration of the project.

An energy method was used to determine the system friction, a known amount of energy being put into the

unloaded system is then dissipated by friction as the system is brought to rest (the method assumes that the frictional torque remains constant with changing speed).

The energy input to the system was provided by a known mass falling through a measured height. This was done using the driving line. Once the energy had been put into the system, the driving line was disconnected and the system allowed to come to rest. The final velocity of the falling mass as well as the angular rotation of the driving and return pulleys are proportional to the highest speed value reached on the speed monitor. The amount of work done against friction was measured by the distance which the towline travelled in coming to rest from the point at which the driving line disconnected. This was accurately done by inputting the pulses from the driving wheel to a pulse counter, the number of pulses then being proportional to the distance travelled (see Appendix D).

The model was checked for water absorption by weighing the hulls, submerging them for 24 hours and then re-weighing them. No absorption took place.

The speed monitor was checked and calibrated by connecting a frequency pulse generator to the input of the frequency to voltage converter. A linear calibration curve was obtained for the designed speed range of the device (see Appendix B).

Extra ballast was added to each hull so that both hulls floated exactly on a grid line. The total weight of the hulls, ballast and supporting structure was then determined and recorded. This was taken as the model displacement and was kept constant throughout the duration of the project.

An alignment jig was constructed to ensure correct and repeatable alignment of the hulls. The initial tests showed, however, that although the hulls were aligned, the model was pulling slightly to one side or the other, depending on the speed of the model, and that the amount of pull increased with increasing separation of the hulls. The setup of the speed timer photo switches was such that the space between the transistor and l.e.d. was only 20 mm, so the model could not deviate more than 10 mm either side of the centre line between the driving and return pulleys.

The pull was due to the hulls not being exactly similar in shape and it was found that by shifting ballast from one hull to the other (which had the effect of slightly increasing or decreasing the displacement and hence drag of the hulls), the model could be made to move in a straight line. The amount of ballast which was moved between the hulls was never more than 30 g, and so did not affect the trim of the hulls nor the overall displacement.

Ideally, the basic aim of the accelerating mass was to bring the model up as close to the required speed in as short a distance as possible, to allow more distance for the speed to asymptote to its exact value before the end of the run, and so result in a more accurate drag result. The initial tests, however, indicated that if the model was accelerated too quickly the model would start to pitch. This could easily be seen on the speed monitor trace. An optimum accelerating distance of 1,5 m was set, leaving a further 9 m of run before the model speed was measured.

The mathematical analysis of the system showed that above a certain value of driving mass an accelerating

mass was no longer necessary since for increasing driving mass the asymptotic value is reached over a smaller distance. This could clearly be seen from the tests where the final speed of the model was the same when run with and without an accelerating mass.

For the purpose of recording the wave profile alongside the hull and calculating the wetted surface area a grid network was drawn on the hull surface. As the model attained its final speed a photograph was taken of the wave profile against the grid. The grid was printed on an A3 sheet of paper on a scale of 2:1. The wave profile from the photograph was then copied onto the A3 paper using the intersections of the wave surface and the grid lines on the photograph. The wetted surface area was then determined using a planimeter. Figure 4.1 shows a half size reduction of the grid network used to calculate the wetted surface area of the hull. Figure 4.2 is a close-up view of the grid network on one of the hulls, while Figure 4.3 is a typical photograph of the wave profiles along the flat and curved sides of the hulls from which the wetted surface area was calculated.

At the end of the run the model was decelerated by the driving mass. The driving line re-wound itself onto the driving pulley, thereby applying a decelerating force.

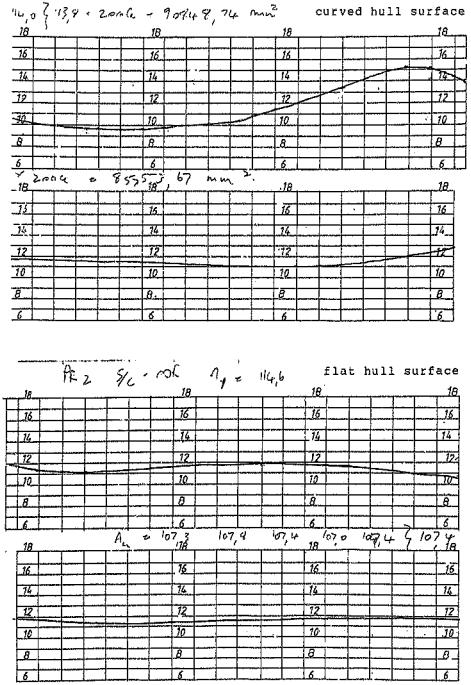

Figure 4.1 A half size reduction of th ork used to calculate wetted sur..

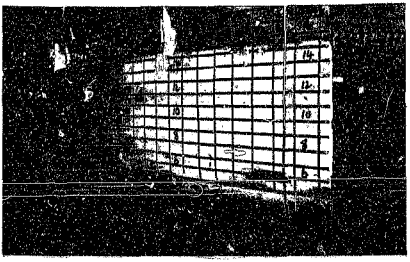

Figure 4.2 Close-up view of a hull

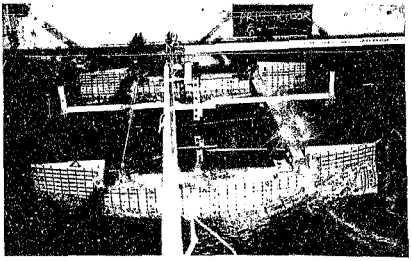

Figure 4.3 Wave profiles on the hulls

4.2 Testing Method

In order to ensure repeatability and accuracy of measurements a set testing method was adopted and used throughout all the tests.

The following were checked on a daily basis before testing commenced;

- tank water circulating pump (switched off)
- correct water level, i.e. distance between towing line and water surface
- settings on all electronic instrumentation

The system friction was also determined and recorded on a daily basis. A change in friction force of more than 0,01 N indicated pulley misalignment or dry pulley bearings. Before the friction was measured the driving pulley was rotated by hand a set number of times to run in the bearings (see Appendix D).

Total model displacement was checked and recorded each time the hull separation was changed. The hulls were wiped clean with a wet sponge to remove any algae or other deposits which might have altered the frictional drag of the model.

The drag value for each test point was set by the driving mass. The initial value for the accelerating mass was then calculated and a run was made using the calculated value (the accelerating distance being fixed at 1,5 m). The resulting speed trace on the chart

recorder was examined to determine whether the model had been under- or over-accelerated and to what extent. The accelerating mass was then readjusted accordingly and a second run was made. This procedure was continued until the correct accelerating mass was determined.

For every run the time interval between the timing switches was recorded on the speed trace as well as the time at which the run took place, and the water temperature at that time, the hull separation and the magnitude of the accelerating and driving masses used were also noted.

The speed trace as well as the measured time interval was used to compare each consecutive run for the determination of the correct accelerating mass and hence the correct time interval for the test point.

The correct accelerating mass was taken as the one which produced the flattest but still increasing speed trace as well as the shortest time interval reading (or highest speed). A very slight over acceleration would result in a lower speed reading than the correct speed due to the model speed having to drop below the correct speed and then asymptote back up to the correct speed. An example of a typical speed trace is given in Figure 4.4. The lighter trace plots the model speed from the beginning of the run, while the darker trace is an amplification of the lighter trace over the constant speed range of the model, and shows a velocity change of 0,005 m/s per chart division.

Once the correct accelerating mass had been determined a final run was made and a photograph of the wave profile taken. Included in the photograph was a photograph number, the hull separation and the Froude

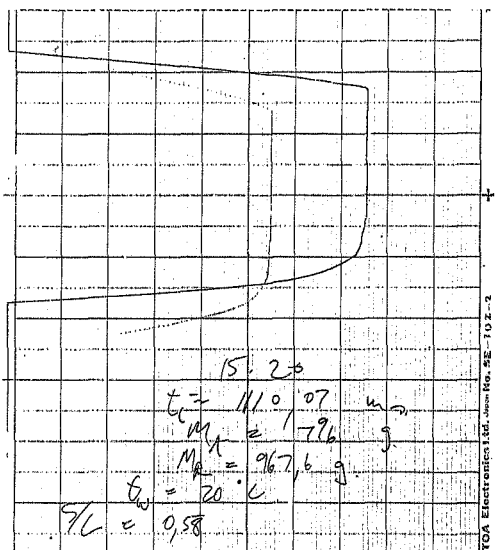

Figure 4.4 A typical speed trace

number.

Once a full set of tests had been completed for a fixed hull separation, their accelerating mass values were used as the initial values for the next set, since for the same value of driving mass there was only a small change in speed for a small change in separation. This considerably reduced the number of runs required to fix a test point. A minimum of two runs was required to fix a test point.

Tests were run at a minimum of half hourly intervals to allow the tank to settle.

4.3 Preliminary Tests

Once the system had been set up and checked, a full range of preliminary tests were run. The tests were used to determine the following:

- repeatability of the measurements
- the Froude number range for the final tests
- the ability of the system to detect a change in wave drag due to a change in hull separation
- the magnitude of the above change

Tests at infinite separation were run first as these were to provide the comparative basis for the other separations. After fixing each test point, it was plotted on a graph of drag versus Froude number, the approximate position of the next point being chosen to

pick up any sharp changes in the resulting curve.

Tests were run through a Froude number range of 0,15 to 0,5 which covers the operating range of most ship types. (High speed destroyers operate at between 0,4 and 0,7 (see Barnaby[9]).)

Two other sets of tests were run at different hull separations. This was done to detect any effects due to wave interference and the magnitude of the effects. These covered the same Froude number range of 0,15 to 0,5.

The results of all three separations were plotted on the same graph as total drag versus Froude number and wave drag coefficient versus Froude number. These are given in Figures 4.5 and 4.6. A dimensionless quantity called the separation/length ratio was used to represent the hull separation. This is defined as:

S/L = the perpendicular distance between the hulls divided by the hull length

The drag versus Froude number plot has a low resolution but it shows the effects of wave interference where the curves representing the separations diverge.

The plot of wave drag coefficient versus Froude number shows clear wave interference effects; in general, adverse effects below Fn = 3 and beneficial effects above Fn = 3.

The actual hull separation at infinity and at S/L = 0,81 was the same except that at infinity the curved sides of the hulls faced outwards while at S/L = 0,81 they faced inwards. At low speeds the curves for S/L = infinity and S/L = 0,81 are similar due to the large

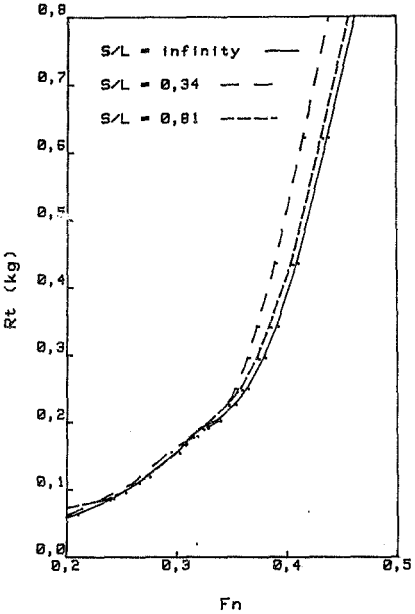

Figure 4.5 Total drag versus Froude number

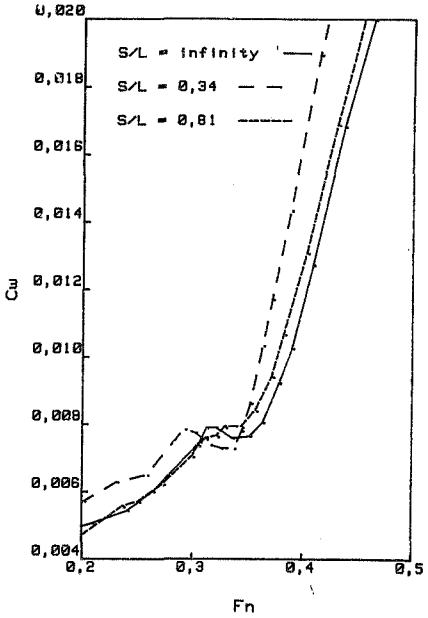

Figure 4.6 Wave drag coefficient versus Froude number

separation and low wave making, while at higher speeds where wave making becomes dominant, the two curves are distinctly separate. This indicates the effectiveness of the flat sides of the hull in producing a small wave system as compared to the curved sides and justifies the nomenclature "infinite" even though the actual hull separation was finite.

The large difference in the curves at S/L = 0,34 and S/L = infinity indicates wave interference effects, even at low speeds, and the ability of the gravity dynamometer and measuring system to detect these effects.

The curves also indicate that major beneficial wave interference effects take place in a Froude number range between 0,29 and 0,37. The results do indicate possible beneficial effects occurring at around Fn = 0,25 which could show up at other S/L ratios. However, it was decided that only the higher speed range would be investigated for the following reasons:

- accuracy and repeatability are reduced at lower speeds due to possible laminar or transitional flow effects and the reduced magnitude of the variables being measured

- the overall effects of interference will be larger at higher speeds, due to the increase in wave making with speed

4.4 Repeatability Tests

Repeatability tests were run at three drag values, covering the proposed speed range i.e. at the beginning, middle and end of the range. At each drag

value seven runs were recorded all using the same driving and the same correct accelerating mass. The tests were all run at infinite separation with the hulls being loosened and then re-aligned after every run. The repeatability tests are detailed in Appendix G.

A statistical analysis was carried out on the results to determine the repeatability of the tests and to determine the expected errors in speed reading and wetted surface area as the errors in these quantities are more of a random nature and are difficult to assess.

A 95 per cent confidence limit was used to fix the error limits, i.e. 1 chance in 20 that the error will lie outside of the limits. The worst error in speed out of the three sets of tests was found to be 0,4 per cent and also 0,4 per cent for the wetted surface area.

This error in speed does not include the possibility that the model could have been slightly over or under accelerated. However, using the formula for the calculation of the percentage error in speed due to not using an accelerating mass the error in speed at the beginning of the test speed range was found to be 1,3 per cent, decreasing to 1,2 per cent in the middle of the range and to 0,5 per cent at the end of the range.

Although approximate, these results do indicate that even without an accelerating mass the model speed will be extremely close to its correct asymptote value by the end of the run and so it can be assumed that with the techniques used to determine the correct accelerating mass there would be negligible speed error due to under- or over-acceleration.

For the three sets of tests the maximum possible error and the most probable error in wave drag coeficient were calculated. The maximum possible error ranged from 1,3 to 2,8 per cent, while the most probable error ranged from 0,8 to 1,6 per cent (see Appendix G).

Examination of the plot of wave drag coefficient versus Froude number at a Froude number of 0,32 shows a change in wave drag coefficient between S/L = infinity and S/L = 0,34 of about 10 per cent, as compared to an error of 1,6 per cent in wave drag coefficient. This clearly indicates the ability of the system to detect a change in wave drag.

4.5 Final Tests

Final tests were carried out over a S/L range from 0,81 to 0,18. For each set of tests, the same driving mass values and spacing of driving mass were used, allowing for easy comparison between two separations, i.e. for the same value of drag different speed readings were obtained at different separations.

Ideally, for the same speed value different drags should be obtained for different separations, but this is not directly measurable with a gravity system. However, once the results are plotted, equations can be derived to fit the points and different drags can then be compared for the same speed.

The results of the preliminary tests were used as a starting point to fully investigate the effects of interference from an infinite separation (at which no interference occurs) to an almost zero separation.

4.6 Results Processing

In order to be able to effectively analyse and observe the effects of wave interference, it is important to be able to compare two different separations where the model is running at the same speed and then examine the resulting change in the wave drag coefficient or the wave drag.

Due to the nature of a gravity dynamometer, the only quantity which can be set is the total drag of the model, all other quantities being dependent on this. This makes comparisons difficult, since all other variables will have to be compared to the total drag, whereas the quantities of interest are the comparisons between the wave drag and wave drag coefficient with speed and separation.

Reasonable comparisons can be made by plotting Cw or Rw against Fn for the various separations on the same axes, but a far more satisfactory result is obtained by deriving an equation for the relationship between Cw, (or Rw) and Fn for each separation. Then, for a given Fn, a quantitative difference in Cw, (or Rw) can be obtained for any two separations. In particular, the difference in Rw between a given separation and an infinite separation can be obtained for any Fn. Conversely, the difference in Rw between two Fn values can be obtained for any separation.

All results calculations, interpolations and graph plots were done on the Hewlett Packard 2000 Computer. For each set of tests, Cw and Rw were calculated and a spline curve fitted to the relationship between Cw and

Fn as well as Rw and Fn. The equations which were used for the calculations are given in Appendix C.

Examination of the distribution of test points on the plot of Rw against Fn showed that the distribution of test points was sufficiently close and continuous so as to justify the fitting of a curve as well as the accuracy in the use of intermediate points on the curve.

A Fn range between 0,30 and 0,37 was set for the following calculations. For each separation, at a given Fn, Rw was divided by Rw at infinite separation at the same Fn. The notation Rwin is used to define the Rw at infinite separation. The same was done for Cw.

The interference ratio, Rw/Rwin (or Cw/Cwin), was plotted against Fn, each curve representing a separation. Also, the interference ratio was plotted against S/L, each curve representing a particular value of Fn.

5 DISCUSSION AND CONCLUSIONS

5.1 Accuracy of Tests and Calculations

The method used for the determination of the overall system friction of the gravity dynamometer did not take into account the increase in frictional torque due to the loading on the bearings while the model was being towed, nor the increase in friction due to the increase in towline tension as the towline moved over the driving pulley. The frictional torque in the bearings was calculated at maximum and minimum test loads and was found to be negligible. The change in system friction due to the movement of the loaded towline over the driving pulley was neglected, it being difficult to determine. It does not affect the results however, due to their comparative nature.

Unloaded system friction tests (see Appendix D), gave not only a quantitative value of drag, but served also as a check on any deviations in the system drag due to misalignment, dirty or dry bearings. Error calculations using the above method indicate an accuracy of 1 per cent in system drag measurement, which is more than adequate, since the accuracy limit of the dynamometer measuring system was set at 0,01 N. For the duration of the testing period, the system drag settled at an average value of 0,07 N, and did not vary more than 0,01 N either side. This was checked at the beginning and at the end of each testing day. This value of system drag was found to be proportional to the towline tension, the tension being that required to prevent slippage of the towline over the large driving pulley.

The repeatability tests as covered in Appendix G show a maximum error in speed reading of 0,4 per cent (maximum, implying the largest error in speed of the three sets of repeatability tests). This was calculated by taking the statistical error in speed reading as a percentage of the mean value of speed for the seven runs. The error in actual time-interval reading, as measured by the counter-timer, can be considered to be negligible; the timer measuring to 0,01 ms. The distance between the timing switches was 1,0 m, accurate to 1,0 mm, giving an error in actual speed of 0,1 per cent. This error however remained constant for all tests.

Speed traces for each run were used to determine the correct accelerating mass for the test point and to evaluate which terminal model speed should be used for the test point. Two channels were used on the chart recorder for this purpose: one to provide a complete trace of the model speed from zero velocity to terminal velocity and the other to amplify the trace as the model approached its terminal speed. The amplified trace showed a change of 0,5 per cent in model speed per chart division. It was found that the terminal model speed was extremely sensitive to a slight over-acceleration. This produced a terminal speed which is far lower than that due to a slight under-acceleration. This effect is characteristic of a gravity system and can be deduced through further analysis of the equations derived in Appendix B. The technique used to determine the terminal velocity of the model for a given drag mass was to examine the amplified speed trace as well as the recorded terminal velocity and to choose the highest terminal velocity which still had an accelerating speed trace. The mass of the model must be considered when using the above method, since a large model mass might still produce an accelerating

speed trace over the length of run even though it had been over accelerated.

The large wave system generated in the area between the hulls produced a significant change in the wetted surface area of the hulls as compared to their static wetted area. This can be seen in Figure 5.1. The grid system used to determine the wetted area had a 20 mm spacing between vertical lines and a 10 mm spacing between horizontal lines. This was due to the larger changes in slope of the wave profile occurring in the vertical direction as compared to the horizontal direction. The error in the calculation of wetted surface area is listed in the results of the repeatability tests (see Appendix G). A separate photograph was taken for each of the seven runs at constant drag, and the resulting wetted surface calculated. The largest error in wetted surface as determined from the photographs, calculated as a percentage of the mean, was 0,4 per cent. This overall statistical error includes all errors due to the transferance of the wave profile from the hull to a photograph and then to the two-dimensional grid, as well as the error in using a planimeter to measure the resulting wetted surface.

The Reynolds number range over which the tests were run was from $0{,}5 \times 10^6$ to $0{,}9 \times 10^6$, below the limit of 10×10^6 given in Birt[10] and Todd[4], for use without artificial stimulation. The conventional trip wire method of turbulence stimulation was used as given by Todd[4] and Allan[12], and it was assumed that this was sufficient to ensure turbulent conditions for all the tests. Laminar flow conditions are a major problem in small model tests and it is extremely difficult to predict or detect. The results of the repeatability tests would seem to indicate that at least steady state

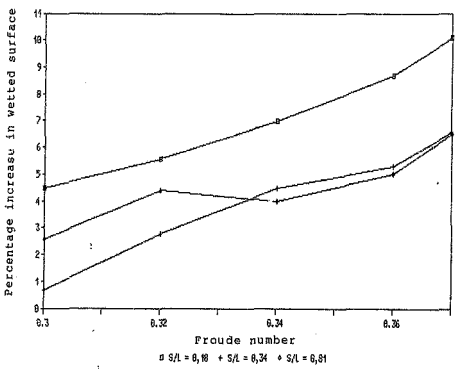

Figure 5.1 Percentage increase in wetted surface versus Froude number

flow conditions were prevalent over the test speed range. Also the resistance ratios used to compare the drag at a specific separation with the drag at infinite separation would effectively annul any error in frictional drag coefficient due to laminar flow, assuming that the flow conditions at a given speed were the same for all separations, be they laminar or turbulent.

Figure I1 in Appendix I gives the expected increase in wave resistance due to testing in a tank of limited depth for a given speed-tank depth ratio. The speed-tank depth ratios for the range of speeds tested all lie along the X-axis, indicating no shallow water effects. The interference ratios would again override any effects due to shallow water (see Appendix I).

Wall effects are not overridden by the interference ratios, since the ratios are a comparison between some separation and an infinite separation, each representing a different distance from the tank wall, and hence indicating a different wall effect. The worst case was at infinite separation, where the model was running closest to the wall at the highest test speed. The wall effect at this separation was calculated using Figures I2 and I3, and it was found that the influence of the wall would produce an increase in measured resistance of just under 2 per cent. This must be compared to the other extreme, where the model was running furthest from the wall, i.e. at the smallest separation. The same test speed was used since the interference ratios are based on equal speeds. For this case the influence of the wall was negligible, giving an error in interference ratio of just under 2 per cent. In general, beneficial wave interference effects occurred in the middle of the speed range and in the middle of the separation range.

It is thus more sensible to compare wall effects at infinite separation with separations in the middle of the separation range, both at a speed in the middle of the speed range. At infinite separation, the error due to the wall is 0,5 per cent, and at a S/L ratio of 0,34 the error is also 0,5 per cent, giving a nett error in interference ratio of zero per cent. These calculations are based on the results of a series of tests to determine the influence of the tank wall on the resistance of a wide variety model shapes, taken from Comstock and Hancock[11], and are considered to be applicable to any tank with a similar cross-section i.e. a breadth to depth ratio close to two.

The results of these calculations are shown in Figure 5.2. Although approximate, they show that the effect on total resistance was relatively small due to the model being in close proximity to the wall, even at small separations and high speeds.

As mentioned earlier, the original drag measurement system which was installed on the tank was a production model towing carriage (see Chapter 3.2) designed for very basic demonstrations of ship model principles. It was felt however that the system could be modified somewhat in order to obtain more accurate and reliable results. Once the system had been installed, it became clear that stiffness problems would not be solved without major re-design of the whole system.

The advantages and disadvantages of a gravity system over a carriage are discussed in Chapter 3.3, the major disadvantage being that the system cannot measure speeds at which the resistance is decreasing with increasing speed. This means that any portion of the drag versus speed curve for a particular hull which should have a negative slope for increasing speed,

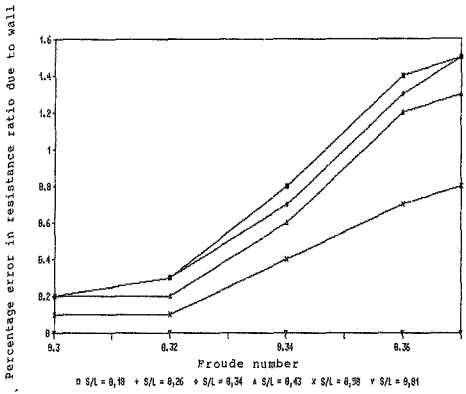

Figure 5.2 Percentage error in resistance ratio due to wall versus Froude number

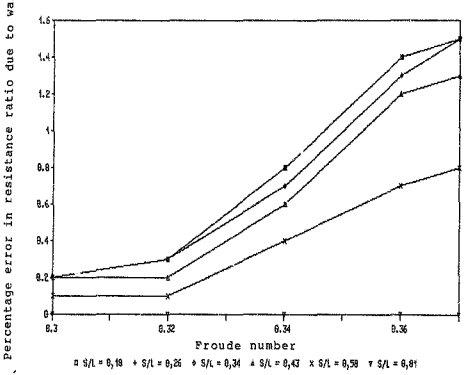

Figure 5.2 Percentage error in resistance ratio due to wall versus Froude number

would instead exhibit zero slope over that speed range. Whether or not this effect occurs depends entirely upon the characteristics of the particular hull being tested, and may prove to be problematic. This again would depend on the magnitude of the negative slope and the magnitude of the speed range over which it occurs. A sufficient amount of test points are required so as to be able to detect the occurrence of any such areas on the total drag versus speed curve. The test results which were obtained for the particular hull used in this poject showed that the curves of total drag versus speed all exhibited increasing total drag with increasing speed for the range of separations tested.

5.2 Effects of Wave Interference

The effects of wave interference are clearly seen in the graphical interpretation of the results, each successive separation producing a different relationship between wave drag and speed.

Figure 5.3 shows the large variation in Cw at different separations as a function of speed. An indication of the region of beneficial interference is seen where the curve of S/L = 0,38 drops below the curve of S/L = infinity. The curves all have the same general shape, i.e. a wave drag which increases exponentially with speed but with a localised maximum and minimum along the curve. The minimum point at infinite separation occurs at Fn = 0,35, while for the other two separations it occurs at Fn = 0,325 and 0,33. The infinite separation curve is seen to be between 90 and 180 degrees out of phase with the other two curves.

Figures 5.4 to 5.7 show the resistance ratio plotted as a function of speed for different separations. The

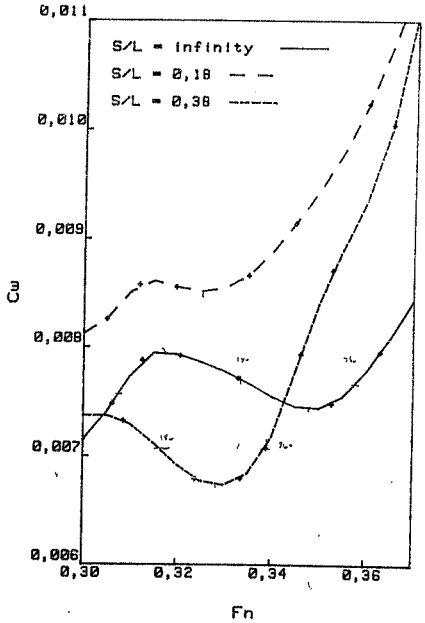

Figure 5.3 Wave drag coefficient versus Froude number

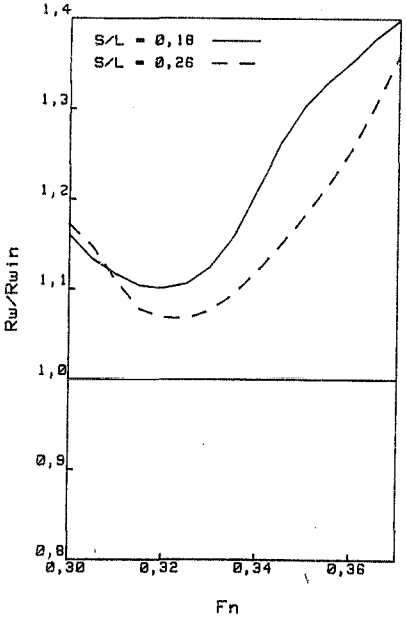

Figure 5.4 Resistance ratio versus Froude number (S/L = 0,18, S/L = 0,26)

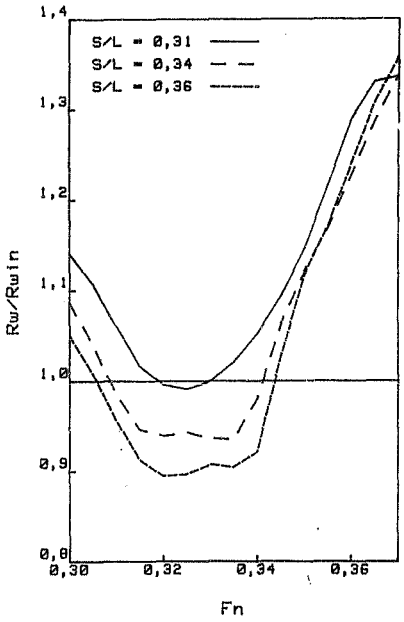

Figure 5.5 Resistance ratio versus Froude number (S/L = 0,31, S/L = 0,34, S/L = 0,36)

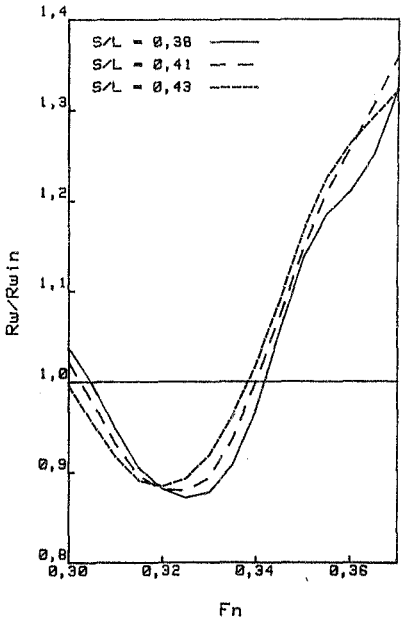

Figure 5.6 Resistance ratio versus Froude number (S/L = 0,38, S/L = 0,41, S/L = 0,43)

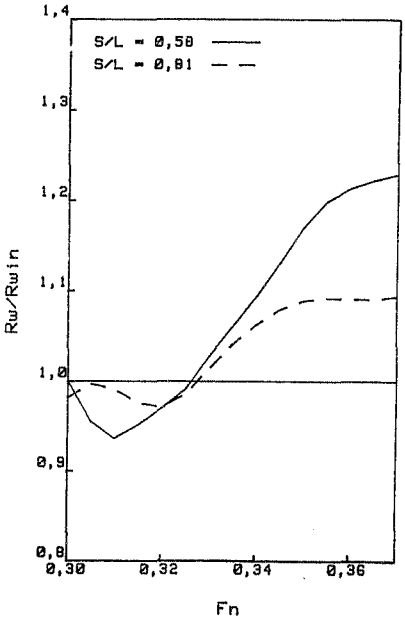

Figure 5.7 Resistance ratio versus Froude number (S/L = 0,58, S/L = 0,81)

horizontal line at a resistance ratio of 1,0 separates the areas of interference; points above the line being adverse wave interference, while those below the line are beneficial. The curves again are all similar.

Each successive separation from S/L = 0,18 to S/L = 0,38 has a lower minimum value than the preceding one. The minimum values then increse with each successive separation. As the separation increases towards infinity, it can be expected that the curves will show less waviness and will eventually become a horizontal straight line through a resistance ratio of 1,0. This is seen by the difference in shape of the curves in Figures 5.6 and 5.7, with the curve at S/L = 0,81 showing the closest approximation to a straight line.

It is interesting to note that the actual hull separation at S/L = 0,81 and S/L = infinity was the same, except that the hulls were reversed, i.e. the flat sides of the hulls were facing each other at S/L = infinity, in contrast to all the other separations. Since the hulls were symmetrical fore and aft, the difference between the curves at S/L = 0,81 and the horizontal straight line shows directly the effect of a change in hull shape on the interference wave pattern between the hulls.

Figures 5.8 to 5.12 show the results plotted as resistance ratio versus S/L ratio for a particular speed. The resistance ratio is seen to drop sharply with increasing S/L ratio in the S/L range of 0,18 to 0,38. For separations larger than this range, the resistance ratio increases but at a slower rate. Figures 5.9 and 5.10 indicate that the optimum separation lies at a S/L ratio of 0,38 and shows that this will hold for a Fn range of 0,315 to 0,330. At this separation a Fn = 0,330 gives the lowest

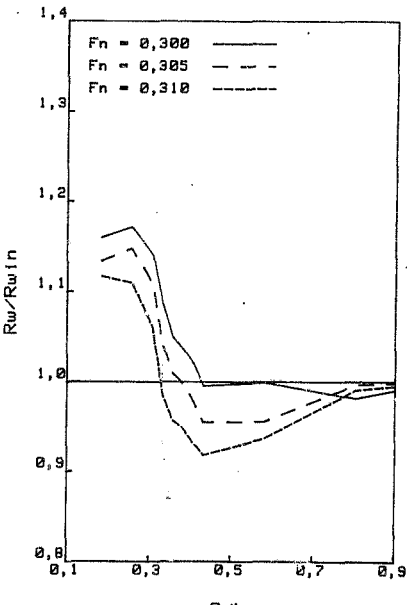

Figure 5.8 Resistance ratio versus separation/length ratio (Fn = 0,300 to 0,310)

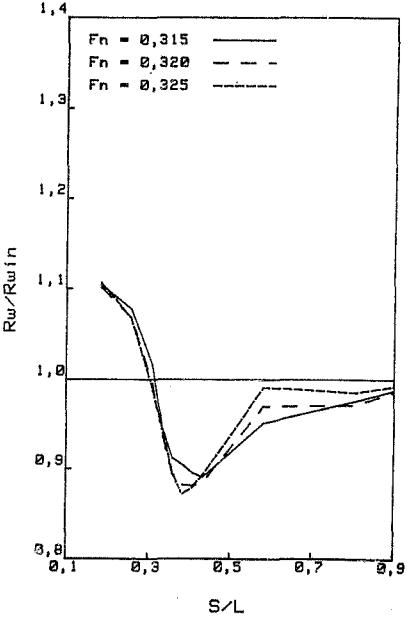

Figure 5.9 Resistance ratio versus separation/length ratio (Fn = 0 to 0,325)

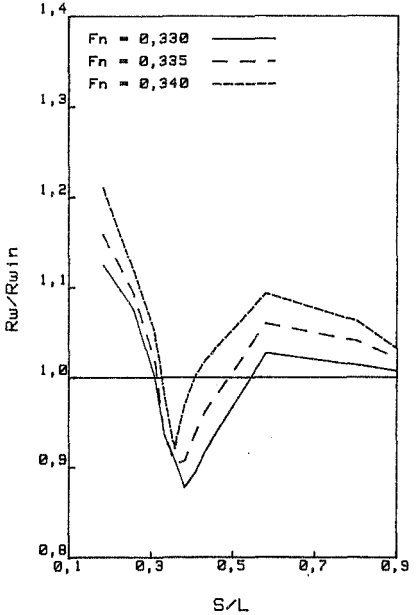

Figure 5.10 Resistance ratio versus separation/length ratio (Fn = 0,330 to 0,340)

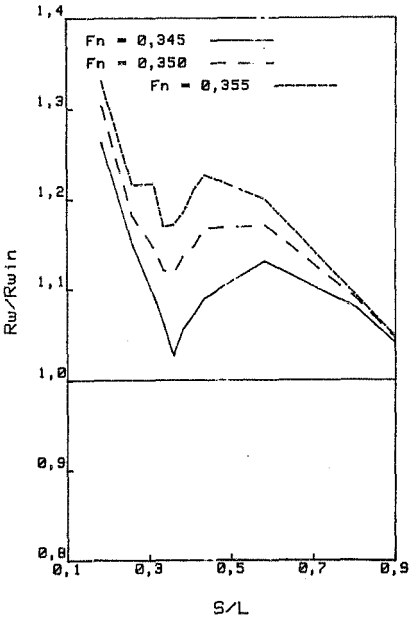

Figure 5.11 Resistance ratio versus separation/length ratio (Fn = 0,345 to 0,355)

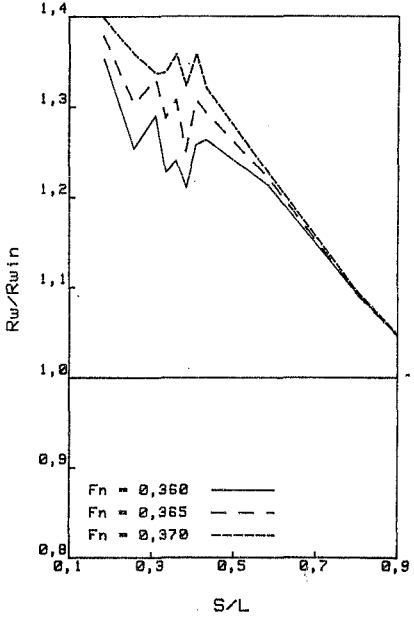

Figure 5.12 Resistance ratio versus separation/length ratio (Fn = 0,360 to 0,370)

resistance ratio of all the separations and speeds tested. At a slightly smaller hull separation, i.e. S/L = 0,36, a larger speed range can be used while S/L = 0,34 gives the largest optimum operating speed range.

Figures 5.11 and 5.12 show that adverse interference exists for all separations when the hulls are run at a Fn greater than 0,34.

It can be deduced that at a S/L ratio smaller than 0,18, the resistance ratio for all speeds will continue to increase, and should theoretically attain a maximun value of two at a separation of zero. This would be the point where a single hull would be running at double its original displacement. At small separations it can be expected that boundary layer interference will take place, producing a variation in skin friction drag. (It was assumed throughout that all separations were large enough to have no boundary layer interference and hence all interference effects are due to wave-making.)

The results can be compared with values calculated by Everest[3]. These are shown in Figures 5.13 and 5.14. (In these two Figures, L is in feet and V is in knots.) Everest used the method derived by Eggers[2] but used measured wave properties of the individual hulls for the calculation of the interference data. The Eggers method uses a mathematically defined hull shape and then calculates the interference data from first principles. By using measured wave properties, Everest eliminated the mathematical difficulties and approximations required to accurately represent the hulls. (Note that the hull separation S was defined here as being the distance between the centreplanes of the hull whereas the separations for this project were taken as the shortest distance between the hulls.)

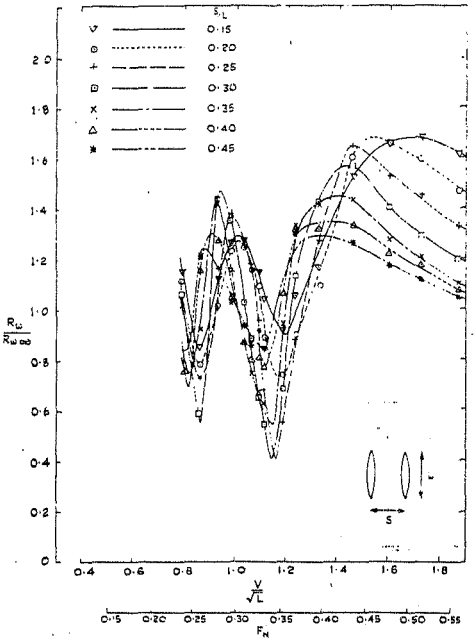

Figure 5.13 Predicted resistance ratio versus Froude number (Everest[3])

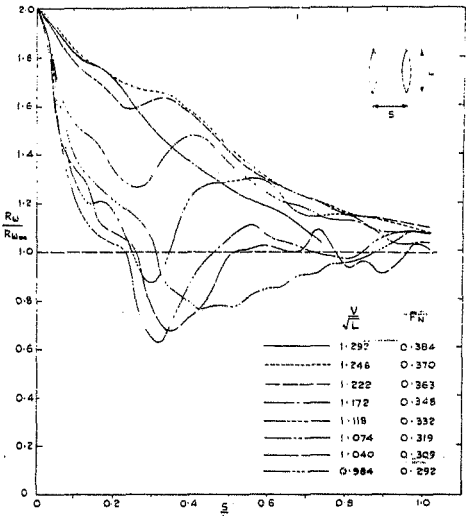

Figure 5.14 Predicted resistance ratio versus separation/length ratio (Everest[3])

Conversion of the S/L ratios from the Everest tests to those of this work requires the subtraction of a factor of 0,1. The Everest tests used the experimentally determined wave properties of a standard test hull for his calculations and so the interference data should differ somewhat from the results of this project, although similar trends are evident.

The Everest S/L ratios referred to in the following text have been modified to accord with those of this work. Comparing Figure 5.14 with Figures 5.8 to 5.12, it is seen that the optimum separation lies at a S/L ratio of about 0,4, which is far smaller than than the optimum obtained here. Also the magnitude of the resistance ratio at the optimum separation differs from 0,52 to 0,87, meaning a saving in wave drag over infinite separation of 48 per cent for the Everest results compared to 13 per cent. This large difference is possibly due to the difference in hull shapes tested. The Everest hulls had waterlines which were parabolic in shape, thus having a more parallel middle body and a sharper change in curvature towards the bow than the model used for this work. This would produce a more separated and stronger bow and stern wave system. The occurrence of the optimum separation point at a small hull separation would mean that the interference wave system is large (wave magnitude decreases with distance from the hull), and so the magnitude of the interference effect would also be large, be it adverse or beneficial.

5.3 General

Chapter 5.1 dicusses the overall tank setup and measurement system with a view to determining its accuracy, limitations and characteristics as well as

its applicability to the specific wave interference tests for which it was used. The use of a gravity system requires an understanding of its characteristics and limitations and this will determine the type of project for which it can be used. Appendix B contains an analysis of a general gravity system.

In general, a gravity dynamometer system, in spite of its simplicity and high accuracy, is not particularly suited to tests where wave drag is being examined due to the inability of the system to measure speeds where the total drag is decreasing with increasing speed. In the case of this project, this effect may have occurred and will have reduced the magnitude of beneficial interference i.e. possibly a greater saving in wave drag than was measured. This would be another possible explanation for the large difference in the measured interference ratio for these tests as compared to those of Everest[3].

The overall results which were obtained using the system show that accurate measurements are attainable with a small towing tank and small models.

5.4 Recommendations for further work

Key questions arising out of this work are as follows:

- To what extent are double hulls used in South Africa ?
- Is there a way of determining which hull shapes would be more conducive for use in a double hull configuration in terms of the basic hull shape factors ?

- How would actual differing sea conditions affect the extent of interference and hence performance ?

- Is there scope for double hulls in the field where wind power would be used as a means of energy saving (in view of their high stability) ?

Many techniques have been developed which have made the mathematical prediction of hull performance easier and more accurate. The development of computer software for these applications would make this task far easier and would open up many more avenues for further research.

A suggestion for a fourth year design project would be to develop a mechanised trolley system which would be as accurate as, or more accurate than, the present gravity dynamometer and have the capability of achieving planing speeds with large models.

Another suggestion for a project would be to calculate the interference data for the particular hull used here and to compare the calculated and experimental results.

REFERENCES

1. Bunt, E.A. and Wells, P. Drag of a model Busemann Biplane Catamaran, **Educational Fluid Mechanics**, 1971, no. 7, pp. 8.

2. Eggers, K.C. Resistance Conditions of Two-Body Ships, **B.S.R.A. Translation 1860.**

3. Everest, J.T. [illegible] Research on the Hydrodynamics of Catamarans and Multi-Hulled Vessels in Calm Water, **N.E.C.I.E.S.**, May 1966.

4. Todd, F.H. The Fundamentals of Ship Model Testing, **S.N.A.M.E.**, April 1951, pp. 107-137.

5. Stoker, J.J. ed, **Water Waves**, New York: Interscience Publishers, 1957, pp. 237.

6. Michell, J.H. The Wave-Resistance of a Ship, **London, Philosophical Magazine**, 1898, pp. 106-123.

7. Havelock, T.H. Wave Resistance: The Mutual Action of Two Bodies, **London, Royal Society Proceedings**, 1936, pp. 460-471.

8. Shiells, R.T. A Skin Friction Determination using Wall-Sided Models of Great Draught, **R.I.N.A.**, March 1953, pp. 280-304.

9. Barnaby, K.C. ed, **Basic Naval Architecture**, London: Hutchinson's Scientific and Technical Publications, 1954.

10. Birt, D.P. ed, **Ship Model Testing**, Tuckahoe N.Y.: John de Graaf Inc., 1970.

11. Comstock, J.P. and Hancock, C.H. The Effect of Size of Towing Tank on Model Resistance, **S.N.A.M.E.**, vol. 50, 1942, pp. 149-184.

12. Allan, J.F. Effect of Laminar Flow on Ship Models, **R.I.N.A.**, August 1949, pp. 107-137.

13. Re[illegible].C., Prau[illegible] and Sherwood, T.K. 3rd ed. **Properties of Gases and Liquids**, New York: McGra[illegible] 1977.

14. Wood, W.G. and Martin, D.G. ed, **Experimental Method: a guide to the art of experiment for students of Science and Engineering**, Athlone Press, 1974.

APPENDIX A

Preliminary Error Analysis

The required variables which have to be calculated are the wave drag coefficient Cw and the wave resistance Rw. For the error analysis, Cw was set up as a function of all the variables which were required to be measured:

$$Cw = Ct - Cf$$

$$= (2gRt/\rho Sv^2) - (0,455/(\log Re)^{2,58})$$

The Reynolds number Re is affected by two variables other than v, namely water temperature t, and kinematic viscos y v, which itself is a function of temperature. In order to reduce the complexity of the analysis, the error in Re was determined separately and then incorporated into the error of Cw.

The following differential method was used: a dependent variable y is related to several independent variables x_i by a known function F:

$$y = F(x_1, x_2 \ldots\ldots\ldots x_n)$$

The error in y, namely dy, is then:

$$dy = (DF/Dx_1)dx_1 + (DF/Dx_2)dx_2 + \ldots\ldots\ldots + (DF/Dx_n)dx_n$$

In the extreme case where the signs of the terms are taken in the worst possible combination, dy represents the maximum possible error. A more realistic error is obtained by a root mean square process:

$$\overline{dy} = \sqrt{(((DF/Dx_1)dx_1)^2)+.....+(((DF/Dx_n)dx_n)^2)}$$

Applying the above to Re we get:

$$\overline{dRe} = \sqrt{((Ldv/\nu)^2+(\nu Ldv/\nu^2)^2)} \qquad (A1)$$

And to Cw:

$$\overline{dCw} = \sqrt{((2gdRt/\rho Sv^2)^2 + (2gRtdS/\rho S^2v^2)^2 + (4gRtdv/\rho Sv^3)^2 + (0,5099dRe(logRe)^{-3,58}/Re)^2)} \qquad (A2)$$

To Rw:

$$\overline{dRw} = \sqrt{((dRt)^2 + (0,455\rho v^2 dS/2g(logRe)^{2,58})^2 + (0,455\rho SvdV/g(logRe)^{2,58})^2 + (0,5099\rho Sv^2 dRe(logRe)^{-3,58}/2gRe)^2} \qquad (A3)$$

Error Calculations

ν is a function of temperature. The maximum possible error in water temperature is 0,5 °C. ρ changes only slightly with temperature and so is taken as remaining constant.

at 21,4 °C, ν = ,734x10^{-7} m^2/s.

at 21,9 °C, $\nu = 9{,}621 \times 10^{-7}$ m^2/s.

therefore $d\nu = 1{,}13 \times 10^{-8}$ m^2/s.

Assume an error of 0,5 per cent in v at an average value of 1,0 m/s. This gives:

$dv = 0{,}005$ m/s.

Therefore at a model length of 0,8 m:

$\overline{dRe} = 10614$

The variable which affects the error in Re the most is v.

The variables used in the following analysis were test results from a 4 ft model, running at a Fn of 0,6 taken from Barnaby[9].

$L = 6{,}04$ m

$S = 3{,}77$ m^2

$v = 4{,}58$ m/s

$Rt = 202{,}1$ N

Errors of 0,5 per cent for Rt and v were taken, and 1 per cent for S. This gave:

$\overline{dCw} = 0{,}0000717$

The calculated Cw was 0,00255, giving an error in Cw of 2,8 per cent.

$\overline{dRe}$ had virtually no effect on $\overline{dCw}$, while dRt and dv had the largest effect. Although the actual model to be used for testing is smaller than the one used in this analysis, requiring the measurement of smaller quantities, a gravity dynamometer system has the advantage of high accuracy in drag and speed measurement and so the error in Cw can be taken as being somewhat conservative.

APPENDIX B

Analysis of the Gravity Dynamometer System

The following analysis is based on the fact that a body moving in a viscous fluid experiences a resisting force which is proportional to its velocity raised to some power. As a first approximation it can be assumed that a model or ship moving in water will have a drag force which is proportional to v^2. Thus we can write:

$$Fr = Kv^2 \qquad (B1)$$

where:

Fr = the force resisting motion or the drag force

K = a constant

A pulley system is schematically represented in Figure B1.

Defining the following:

ma = accelerating mass

mr = driving mass

mb = mass of model

mw = mass of driving and return pulleys

a = acceleration of the system

α = angular acceleration of pulleys

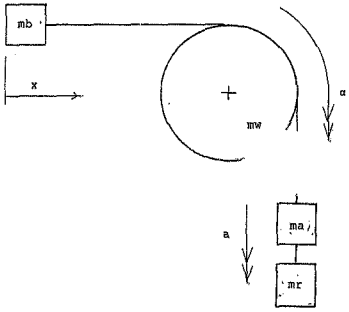

Figure B1 Schematic view of a pulley system

x = distance from the start of the run

Applying Newton's Second Law to the accelerating system:

$$dv/dt(-mw-2mb-2ma-2mr) = 2Kgv^2-2gma-2gmr \qquad (B2)$$

Let:

$$A = -2mw-2mb-2mr-2ma$$

$$B = -2Kg$$

$$C = -2gmr-2gma$$

$$mt = ma+mr+mb+mw$$

Solving the differential equation gives:

$$v^2 = C/B(1-e^{(-2Bx/A)}) \qquad (B3)$$

The limiting velocity which the model attains after an accelerating distance s is:

$$vlim^2 = (ma+mr)/K \qquad (B4)$$

Substituting (B4) into (B3) gives:

$$(mr+ma)/mr = 1/(1-e^{(-2Kgs/mt)}) \qquad (B5)$$

Let:

$$D = 2Kgs/mt$$

and substitute the Maclaurin's Expansion for e^D in (B5). Neglecting fourth order terms and higher we get:

$$ma = v^2mt/(2gs(1+(Kgs/mt)+2/3(Kgs/mt)^2)) \qquad (B6)$$

x = distance from the start of the run

Applying Newton's Second Law to the accelerating system:

$$dv/dt(-mw-2mb-2ma-2mr) = 2Kgv^2-2gmw-2gmr \qquad (B2)$$

Let:

$$A = -2mw-2mb-2mr-2ma$$

$$B = -2Kg$$

$$C = -2gmr-2gma$$

$$mt = ma+mr+mb+mw$$

Solving the differential equation gives:

$$v^2 = C/B(1-e^{(-2Bx/A)}) \qquad (B3)$$

The limiting velocity which the model attains after an accelerating distance s is:

$$vlim^2 = (ma+mr)/K \qquad (B4)$$

Substituting (B4) into (B3) gives:

$$(mr+ma)/mr = 1/(1-e^{(-2Kgs/mt)}) \qquad (B5)$$

Let:

$$D = 2Kgs/mt$$

and substitute the Maclaurin's Expansion for e^D in (B5). Neglecting fourth order terms and higher we get:

$$ma = v^2mt/(2gs(1+(Kgs/mt)+2/3(Kgs/mt)^2)) \qquad (B6)$$

Hence for a given accelerating distance s, the approximate accelerating mass, ma can be calculated from equation (B6).

Examination of equation (B3) shows that without an accelerating mass the model speed will asymptote towards the required velocity vlim and that the difference between the actual velocity v and the required velocity vlim after a certain distance x is dependent on K and mt. Since K, mb and mw are fixed for a particular model and towing system setup, the error in velocity after a length of run x is only a function of mr, i.e. as mr increases, so the error decreases.

With ma = 0, (B3) becomes:

$$v^2 = mr(1-e^{(-2Kgx/mt)})/K \qquad (B7)$$

Substituting (B4) into (B7) we get:

$$v^2/vlim^2 = (1-e^{(2Kgs/mt)}) \qquad (B8)$$

Let:

$$n = v/vlim \qquad (B9)$$

The percentage error in velocity due to not using an accelerating mass is then:

$$100(n-1)$$

APPENDIX C

Sample Calculations

The following are the calculations required to determine the wave drag and wave drag coefficient for a test point. The measured quantities were:

$Rt = 0,623$ N

$v = 0,5865$ m/s

$t = 25,3$ °C

$S = 0,3585$ m^2

Kinematic viscosity

An equation relating the kinematic viscosity of water to its temperature was derived from values given in Reid[13]:

$$\nu = a_4t^4+a_3t^3+a_2t^2+a_1t+a_0$$

where:

$a_4 = -2,2x10^{-7}$

$a_3 = 9,93x10^{-6}$

$a_2 = 4,5x10^{-4}$

$a_1 = -4,72x10^{-2}$

$$a_0 = 1,7253$$

t is the water temperature in degrees centigrade and ν is in centistokes. At 25,3 °C:

$$\nu = 0,8909 \times 10^{-6} \text{ m}^2/\text{s}$$

Reynolds number

$$Re = VL/\nu$$

For a length of model of 0,8 m:

$$Re = 5,269 \times 10^5$$

Skin friction coefficient

The Prandtl-Schlichting skin friction formulation used to determine Cf was taken from Barnaby[9]:

$$Cf = 0,455/(\log(Re))^{2,58}$$

$$= 5,054 \times 10^{-3}$$

Total resistance coefficient

$$Ct = 2Rt/\rho SV^2$$

ρ was taken as being constant over the test temperature range as it varies by only 0,1 per cent, and so an average value of 997,8 kg/m^3 was used. This gives:

$$Ct = 1,012 \times 10^{-2}$$

Wave resistance coefficient

The wave resistance coefficient Cw, is the difference between Ct and Cf:

$$Cw = Ct - Cf$$

$$= 5,067 \times 10^{-3}$$

Wave drag

$$Rw = Cw \rho S v^2/2$$

$$= 0,3119 \text{ N}$$

APPENDIX D

Determining System Friction

The principle of conservation of energy was used to determine the overall system friction of the gravity dynamometer. The method, however, only gives the friction of the unloaded dynamometer and does not account for the increased frictional torque in the bearings due to load, nor the friction due to the increase in towline tension as the towline moved over the driving pulley.

The friction in the bearings due to load can be calculated separately using a formula given in the bearings specifications manual, but this is negligible relative to the system friction.

Friction due to the increase in towline tension under load is difficult to determine and was not considered.

Unloaded System Friction

Consider the system represented in Figure D1: a pulley driven by a falling mass, which falls through a given height h.

Assuming that the frictional torque acting on the system remains constant with speed, then by the principle of conservation of energy:

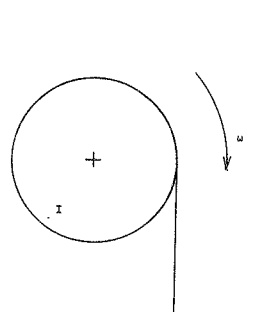

Figure D1 Falling mass driving pulley

(initial energy)

+(energy added) = (final energy)

+(energy removed)

or:

$$mgh = I\omega^2/2+mv^2/2+Tf\theta_i \qquad (D1)$$

where:

I = the mass moment of inertia of the pulley

m = a known mass

ω = angular velocity of the pulley after falling through the height h

V = velocity of the mass after falling through the height h

Tf = the frictional torque

θ_i = the total angle through which the pulley rotates while the mass is falling through the height h

θ_f = the total angle through which the pulley rotates from the instant at which the falling mass disconnects from the system to where the system comes to rest

If the mass is disconnected after falling through the given height and the system is allowed to come to rest under the influence of the frictional torque, then again by the principle of conservation of energy:

$$I\omega^2/2 = Tf\theta_f \qquad (D2)$$

Substituting (D2) into (D1):

$$Tf = (mgh-mv^2/2)/(\theta_i+\theta_f) \qquad (D3)$$

Hence the frictional torque in the unloaded system can be calculated using (D3). A known mass is used to accelerate the system by falling through a measured height, after which the mass is then disconnected and the system is allowed to come to rest.

The driving pulley and mass are used for this purpose and are stopped instantaneously after a fixed distance. The driving line then disconnects and the total number of revolutions of the driving pulley is measured, i.e. proportional to $(\theta_i+\theta_f)$. This was accurately done by connecting the output of the photo-transistor on the driving pulley to a pulse counter, the total number of pulses then being proportional to $(\theta_i+\theta_f)$.

The final velocity of the falling mass is proportional to the maximum velocity reading on the speed monitor.

The resulting frictional drag in the towing line Fd is then:

$$Fd = Tf/r$$

where:

r = radius of the driving pulley

An error in this method occurs due to the pulley in the ceiling not being included in the system after the driving line disconnects, but this will be small

compared to the friction of the towing line over the driving and return pulleys.

Bearing Load Friction

The dominating load on the driving and return pulleys is that due to the towline tensioning mass which was 4,5 kg. The range of driving masses which were used was from 0,8 to 1,7 kg.

Two 6 mm bore F.A.G. self-aligning ball bearings were used per pulley. The manufacturers' catalogue gives a formula for the calculation of the frictional torque of a bearing in terms of the coefficient of friction.

$$u = 2Mf/Fd$$

where:

Mf = the friction torque of the bearing

F = the bearing load

d = the bearing bore

u = the coefficient of friction given as 0,001 6 for a self-aligning bearing with a radial load

The maximum and minimum frictional moments on the driving pulley are thus:

$$Mf_{max} = F_{max}ud/2$$

$$= 5163x0,0016x6/2$$

$$= 25x10^{-5} \text{ N.m}$$

$$Mf_{min} = F_{min} ud/2$$

$$= 4742 \times 0{,}0016 \times 6/2$$

$$= 23 \times 10^{-5} \text{ N.m}$$

The resulting drag on the towline due to the frictional torque is the frictional torque divided by the radius of the driving pulley, which is 126,5 mm. This gives:

$$Fd_{max} = 0{,}002 \text{ N}$$

$$Fd_{min} = 0{,}002 \text{ N}$$

From this it can be seen that the change in loading on the bearings has negligible effect on the bearing frictional drag (within the required accuracy of the tests).

APPENDIX E

Design of the Speed Monitor

The speed monitor operates off the large driving pulley. Holes are drilled through the pulley and a photo-transistor and infrared-emitting diode are mounted on either side of the pulley. As each hole in the pulley passes between the transistor and l.e.d., a voltage pulse is generated. The frequency of the pulses is proportional to the angular velocity of the pulley, which in turn is proportional to the model speed.

The voltage pulses are then passed into a Schmidt trigger which modifies the pulses into a square wave and then to a frequency to voltage converter which converts the frequency change into a voltage change.

The size and spacing of the holes on the large driving pulley are constrained by the switching time of the photo-transistor. A design speed operating range for the gravity dynamometer was set at 0,1 to 2,0 m/s, and this was used to determine the hole sizes and spacing.

The number of holes determines the output frequency range from the photo-transistor and this must comply with the operating range of the frequency to voltage converter. The driving pulley has 128 equally spaced holes lying on a 243 mm diameter, giving one pulse per 6,5 mm model travel. A chart recorder then records the voltage change. Two channels on the chart recorder were used, one which traced the model speed from zero velocity to maximum, while the other amplified the speed trace over the constant speed range.

The amplified signal shows a velocity change of 0,005 m/s per chart division, which is an average change of 0,5 per cent (there are 100 divisions on the chart).

Because the voltage range of the amplified signal lay beyond the voltage range of the chart recorder, a circuit was built which changed the reference voltage so that the constant speed signal occurs within the chart recorder range. The voltage was adjusted using a potentiometer.

For the purpose of determining and checking the system friction, the output from the Schmidt trigger was also fed into a pulse counter.

Calibration of the Speed Monitor

The speed monitor was calibrated in order to check its linearity and to be able to determine the velocity of the falling driving mass for the calculation of the system friction.

For the calibration, a standard pulse generator was connected to the input of the frequency to voltage converter. The frequency of the pulses was accurately measured by a standard frequency meter. The calibration chart is given in Figure B1.

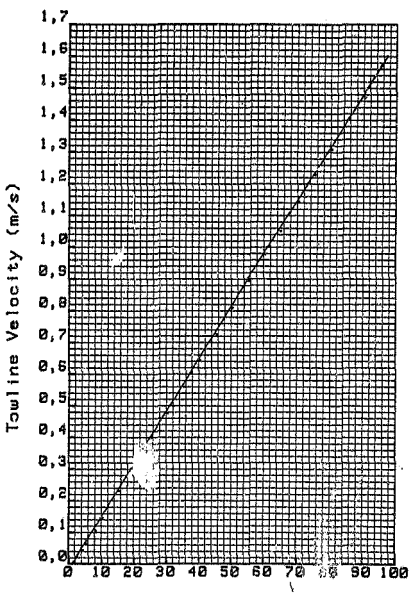

Figure B1 Calibration chart for the speed monitor

Electrical Circuitry

The following pages give the technical data used for the speed monitor system as well as the camera activating circuit.

National Semiconductor

Industrial/Automotive/Functional Blocks/Telecommunications

LM2907, LM2917 Frequency to Voltage Converter

General Description

The LM2907, LM2917 series are monolithic frequency to voltage converters with a high gain op amp/comparator designed to operate a relay, lamp, or other load when the input frequency reaches or exceeds a selected rate. The tachometer uses a charge pump technique and offers frequency doubling for low ripple, full input protection in two versions (LM2907-8, LM2917-8) and its output swings to ground for a zero frequency input.

(Continued on page 9-83)

Advantages

Output swings to ground for zero frequency input

- Easy to use: $V_{OUT} = f_{IN} \times V_{CC} \times R1 \times C1$
- Only one RC network provides frequency doubling
- Zener regulator on chip allows accurate and stable frequency to voltage or current conversion. (LM2917)

Features

- Ground referenced tachometer input interfaces directly with variable reluctance magnetic pickups
- Op amp/comparator has floating transistor output
- 50 mA sink or source to operate relays, solenoids, meters, or LEDs
- Frequency doubling for low ripple
- Tachometer has built-in hysteresis with either differential input or ground referenced input
- Built-in zener on LM2917
- ±0.3% linearity typical
- Ground referenced tachometer is fully protected from damage due to swings above V_{CC} and below ground

Applications

- Over/under speed sensing
- Frequency to voltage conversion (tachometer)
- Speedometers
- Breaker point dwell meters
- Hand-held tachometer
- Speed governors
- Cruise control
- Automotive door lock control
- Clutch control
- Horn control
- Touch or sound switches

Block and Connection Diagrams

Dual-In-Line Packages, Top Views

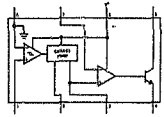

Order Number LM2907N-8
See NS Package N08E

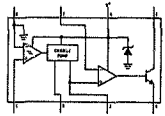

Order Number LM2917N-8
See NS Package N08E

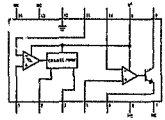

Order Number LM2907J
See NS Package J14A
Order Number LM2907N
See NS Package N14A

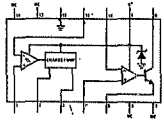

Order Number LM2917J
See NS Package J16A
Order Number LM2917N
See NS Package N16A

MOTOROLA Semiconductors
BOX 2091 • PHOENIX, ARIZONA 85036

MC14093B

Advance Information

QUAD 2-INPUT "NAND" SCHMITT TRIGGER

The MC14093B Schmitt trigger is constructed with MOS P-channel and N-channel enhancement mode devices in a single monolithic structure. These devices find primary use where low power dissipation and/or high noise immunity is desired. The MC14093B may be used in place of the MC14011B quad 2-input NAND gate for enhanced noise immunity or to "square up" slowly changing waveforms.

- Quiescent Current = 0.5 nA typ/pkg @ 5 Vdc
- Supply Voltage Range = 3.0 Vdc to 18 Vdc
- Capable of Driving Two Low-Power TTL Loads, One Low-Power Schottky TTL Load or Two HTL Loads Over the Rated Temperature Range
- Double Diode Protection on All Inputs
- Pin-for-Pin Compatible with CD4093
- Can be Used to Replace MC14011B

McMOS SSI

(LOW-POWER COMPLEMENTARY MOS)

QUAD 2-INPUT "NAND" SCHMITT TRIGGER



L BUFFIX
CERAMIC PACKAGE
CASE 632

P BUFFIX
PLASTIC PACKAGE
CASE 646

ORDERING INFORMATION

MC14XXXB — Suffix Denotes
- L Ceramic Package
- P Plastic Package
- A Extended Operating Temperature Range
- C Limited Operating Temperature Range

MAXIMUM RATINGS (Voltages referenced to V_{SS})

Rating	Symbol	Value	Unit
DC Supply Voltage	V_{DD}	-0.5 to +18	Vdc
Input Voltage, All Inputs	V_{in}	-0.5 to V_{DD} + 0.5	Vdc
DC Current Drain per Pin	I	10	mAdc
Operating Temperature Range — AL Device CL/CP Device	T_A	-55 to +125 -40 to +85	°C
Storage Temperature Range	T_{stg}	-65 to +150	°C

EQUIVALENT CIRCUIT SCHEMATIC
(1/4 OF CIRCUIT SHOWN)

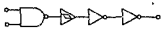

LOGIC DIAGRAM

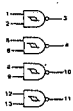

V_{DD} = Pin 14
V_{SS} = Pin 7

This device contains circuitry to protect the inputs against damage due to high static voltages or electric fields; however, it is advised that normal precautions be taken to avoid application of any voltage higher than maximum rated voltages to this high impedance circuit. For proper operation it is recommended that V_{in} and V_{out} be constrained to the range $V_{SS} \leq (V_{in}$ or $V_{out}) \leq V_{DD}$.
Unused inputs must always be tied to an appropriate logic voltage level (e.g., either V_{SS} or V_{DD}).

MOTOROLA
Semiconductors
Avenue General Eisenhower 31023 Toulouse CEDEX – FRANCE

MRD701

PLASTIC NPN SILICON PHOTOTRANSISTORS

. . . designed for industrial processing and control applications such as light modulators, shaft or position encoders, end of tape detectors. The MRD701 is designed to be used with the MLED71 infrared emitter in optical slotted coupler/interrupter applications.

- Economical, Miniature Plastic Package
- Package Designed for Accurate Positioning
- Lens Molded into Package

30 VOLT

PHOTOTRANSISTOR

NPN SILICON

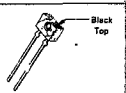

MAXIMUM RATINGS

Rating	Symbol	Value	Unit
Collector-Emitter Voltage	V_{CEO}	30	Volts
Total Device Dissipation @ T_A = 25°C Derate above 25°C	P_D(1)	150 2.0	mW mW/°C
Operating and Storage Junction Temperature Range	T_J, T_{stg}(2)	−40 to +100	°C

(1)Measured with the device soldered into a typical printed circuit board.
(2)Heat Sink should be applied to leads during soldering to prevent case temperature from exceeding 100°C.

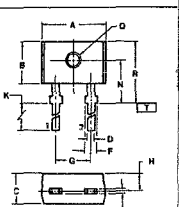

STYLE 2:
PIN 1. EMITTER
2. COLLECTOR

NOTES:
1. DIMENSIONS A, B AND C ARE DATUMS.
2. POSITIONAL TOLERANCE FOR D DIMENSION: ⌖ .25 (0.010) Ⓜ | T | A Ⓜ | E Ⓜ
3. POSITIONAL TOLERANCE FOR D DIAMETER: ⌖ .25 (0.010) Ⓜ | A Ⓜ | B Ⓜ
4. T IS SEATING PLANE.
5. DIMENSIONING AND TOLERANCING PER ANSI Y14.5, 1973.

DIM	MILLIMETERS MIN	MAX	INCHES MIN	MAX
A	3.45	4.80	0.135	0.185
B	2.79	3.30	0.110	0.130
C	2.03	3.18	0.080	0.125
D	0.43	0.56	0.017	0.022
F	1.14	1.40	0.045	0.055
G	2.54 BSC		0.100 BSC	
H	1.52 BSC		0.060 BSC	
J	0.23	0.38	0.009	0.015
K	12.83	13.95	0.505	0.750
N	3.05	3.30	0.120	0.130
R	2.16	2.52	0.030	0.099
T	3.81	4.60	0.150	0.181

CASE 349-01

FIGURE 1 — ANGULAR RESPONSE

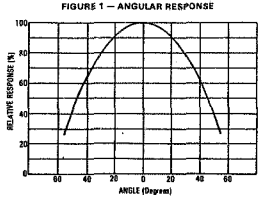

MOTOROLA Semiconductors

Avenue Général-Eisenhower 31023 Toulouse CEDEX – FRANCE

MLED71

INFRARED-EMITTING DIODE

. . . designed for infrared remote control applications for use with the MRD701 phototransistor in optical slotted coupler/interrupter module applications, and for industrial processing and control applications such as light modulators, shaft or position encoders, end of tape detectors.

- Continuous P_O = 2.5 mW (Typ) @ I_F = 50 mA
- Low Cost, Miniature, Clear Plastic Package
- Package Designed for Accurate Positioning
- Lens Molded into Package
- Narrow Spatial Radiation Pattern

INFRARED-EMITTING DIODE

PN GALLIUM ARSENIDE

940 nm

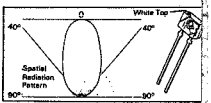

MAXIMUM RATINGS

Rating	Symbol	Value	Unit
Reverse Voltage	V_R	6.0	Volts
Forward Current — Continuous	I_F	50	mA
Total Power Dissipation @ T_A = 25°C Derate above 25°C	P_D(1)	150 2.0	mW mW/°C
Operating and Storage Junction Temperature Range	T_J, T_{stg}	–40 to +100	°C

THERMAL CHARACTERISTICS

Characteristic	Symbol	Max	Unit
Thermal Resistance Junction to Ambient	$R_{\theta JA}$(1)	350	°C/W

(1) Measured with the device soldered into a typical printed circuit board.

Motorola reserves the right to make changes to any products herein to improve reliability, function or design. Motorola does not assume any liability arising out of the application or use of any product or circuit described herein; neither does it convey any license under its patent rights nor the rights of others.

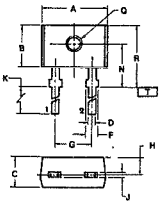

STYLE 1:
PIN 1. CATHODE
2. ANODE

NOTES:
1. DIMENSIONS A, B AND C ARE DATUMS.
2. POSITIONAL TOLERANCE FOR D DIMENSION: ⌖ .25 (0.010) ⓜ -T- A ⓜ C ⓜ
3. POSITIONAL TOLERANCE FOR Q DIAMETER: ⌖ .25 (0.010) ⓜ A ⓜ B ⓜ
4. ⊥ .25 SEATING PLANE.
5. DIMENSIONING AND TOLERANCING PER ANSI Y14.5, 1973.

DIM	MILLIMETERS MIN	MILLIMETERS MAX	INCHES MIN	INCHES MAX
A	3.43	4.60	0.135	0.185
B	2.79	3.30	0.110	0.130
C	2.03	3.18	0.080	0.125
D	0.43	0.56	0.017	0.022
F	1.14	1.40	0.045	0.055
G	2.54 BSC		0.100 BSC	
H	1.57 BSC		0.060 BSC	
J	0.22	0.56	0.009	0.022
K	12.63	19.05	0.505	0.750
N	3.05	3.30	0.120	0.130
Q	0.76	1.52	0.030	0.060
R	3.81	4.68	0.150	0.185

CASE 349-01

FIGURE 1 — TYPICAL INSTANTANEOUS POWER OUTPUT

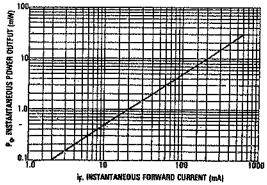

APPENDIX F

Wetted Surface Area and Displacement Calculations

The total wetted surface area of the model was required for the purposes of calculating the wave drag coefficient. The wetted surface area was calculated at the static waterline, W.L. 11 and then from the photograph of the moving model, the change in wetted surface with respect to W.L. 11 was calculated. This was then added to the static wetted surface area.

The model displacement was also calculated at W.L. 11 and compared with the actual model displacement.

Wetted Surface Area Calculation

Simpson's Rule was used for the calculation of the wetted surface of the faired part of the hull, the hull being divided up into segments as shown in Figure F1 (the same size segments were used in the construction of the model, see Appendix H).

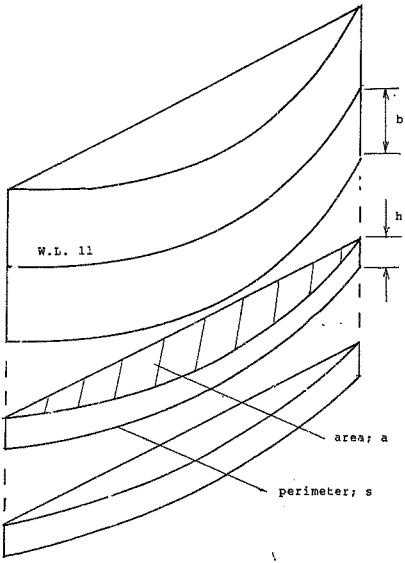

Figure F1 Hull segments

We define the following:

$s_b, s_1 \ldots\ldots s_n$ = perimeter of each hull segment

$a_b, a_1 \ldots\ldots a_n$ = area of each hull segment

B = depth of hull from the static waterline, W.L. 11 to the point at which hull becomes faired

h = depth of each faired segment (all at the same depth)

The surface area of the non-faired part of the hull is:

$S_b = s_b \times B$

$= 1622 \times 45$

$= 73319 \text{ mm}^2$

We define the following:

$s_b, s_1 \ldots s_n$ = perimeter of each hull segment

$a_b, a_1 \ldots a_n$ = area of each hull segment

B = depth of hull from the static waterline, W.L. 11 to the point at which hull becomes faired

h = depth of each faired segment (all at the same depth)

The surface area of the non-faired part of the hull is:

$S_b = s_b \times B$

$= 1622 \times 45$

$= 73319 \text{ mm}^2$

Table F1 Simpson's Rule applied to the hull segments for the calculation of surface area

ordinate	multiplier	s (mm)	function (mm^2)
s_9	1	1600	1600
s_8	4	1604	6414
s_7	2	1606	3211
s_6	4	1610	6438
s_5	2	1613	3226
s_4	4	1616	6465
s_3	2	1619	3238
s_2	4	1620	6482
s_1	1	1622	1622

Therefore the surface area of the faired part of the hull is:

$$S_h = 8,1 \times 38696/3$$

$$= 104480 \text{ mm}^2$$

The total static wetted surface area for both hulls is:

$$S = 2(S_b+S_h)$$

$$= 2(73319+104480)$$

$$= 355598 \text{ mm}^2$$

Table F1 Simpson's Rule applied to the hull segments for the calculation of surface area

ordinate	multiplier	s (mm)	function (mm^2)
s_9	1	1600	1600
s_8	4	1604	6414
s_7	2	1606	3211
s_6	4	1610	6438
s_5	2	1613	3226
s_4	4	1616	6465
s_3	2	1619	3238
s_2	4	1620	6482
s_1	1	1622	1622

Therefore the surface area of the faired part of the hull is:

$$S_h = 8,1x38696/3$$

$$= 104480 \text{ mm}^2$$

The total static wetted surface area for both hulls is:

$$S = 2(S_b+S_h)$$

$$= 2(73319+104480)$$

$$= 355598 \text{ mm}^2$$

Calculation of Model Displacement

Simpson's Rule was again used as above, this time using the area of each segment.

The volume of the non-faired part of the hull is:

$$M = a_b \times B$$

$$= 44646 \times 45$$

$$= 2017994 \text{ mm}^3$$

Table F2 Simpson's Rule applied to the hull segments for the calculation of volume

ordinate	multiplier	a (mm^2)	function (mm^3)
a_9	1	0	0
a_8	4	19930	79719
a_7	2	24371	48741
a_6	4	30198	120790
a_5	2	34837	69674
a_4	4	38438	153753
a_3	2	41314	82627
a_2	4	42896	171583
a_1	1	44646	44646

The volume of the faired part of the hull is:

M_h = 8,1x771532/3

= 2083136 mm^3

The total static volume for both hulls is:

M = 2(M_b+M_h)

= 2(2017994+2083136)

= 8202260 mm^3

The calculated static displacement mass of the model is thus:

D = Mxρ

= 0,008202x997,8

= 8,184 kg

The actual static model displacement was 7,942 kg.

APPENDIX G

Repeatability Tests

Repeatability tests were run at three set values of drag and the variations in speed and wetted surface area were determined and recorded. Seven tests per drag setting were run.

Table G1 lists the results of the repeatability tests which were run at infinte separation.

Confidence limits of 95 per cent were chosen. Wood and Martin[14] gives a formula for computing the limits for a given sample size n and a confidence P.

$$ks = st/n^{0,5} \qquad (G1)$$

where:

t = a tabulated value which is a function of P and n

s = the standard deviation of the readings

ks = the actual error

The formula thus implies that the confidence is P that the true value is within the range m-ks and m+ks, where m is the mean value of the readings. At a confidence of P = 0,95 (95 per cent), and a sample size of n = 7, Wood and Martin[14] lists a value of t = 2,45.

For each test the wave drag and wave drag coefficient were also calculated and the statistical errors for

Table G1 Repeatability test results at infinite separation

test no.	Rt (N)	Fn	S (m^2)	t ($^{\circ}C$)
1	1,536	0,?007	0,3629	24,7
2	1,536	0,3000	0,3645	20,8
3	1,536	0,2994	0,3642	18,7
4	1,536	0,2994	0,3662	18,7
5	1,536	0,2990	0,3672	18,7
6	1,536	0,2982	0,3665	18,5
7	1,536	0,2984	0,3651	18,5
8	1,992	0,3369	0,3672	24,4
9	1,992	0,3330	0,3693	20,8
10	1,992	0,3336	0,3697	18,4
11	1,992	0,3333	0,3700	18,4
12	1,992	0,3334	0,3688	18,5
13	1,992	0,3326	0,3706	18,4
14	1,992	0,3339	0,3702	18,5
15	3,363	0,3905	0,3809	24,0
16	3,363	0,3896	0,3817	20,6
17	3,363	0,3901	0,3823	18,4
18	3,363	0,3896	0,3824	18,4
19	3,363	0,3893	0,3810	18,4
20	3,363	0,3897	0,3809	22,0
21	3,363	0,3909	0,3826	21,8

these quantities also examined.

Applying equation (G1) to the results we get the following errors as listed in Table G2.

Table G2 Errors

	ks			
Rt (N)	Fn	S (m^2)	Cw	Rw (N)
1,536	$8,09x10^{-4}$	$1,40x10^{-3}$	$4,81x10^{-5}$	$5,48x10^{-3}$
1,992	$1,32x10^{-3}$	$1,05x10^{-3}$	$4,57x10^{-5}$	$5,95x10^{-3}$
3,363	$5,29x10^{-4}$	$7,00x10^{-4}$	$5,17x10^{-5}$	$8,82x10^{-3}$

Error Analysis

The statistical errors for speed and wetted surface area given above were used in the error formulae for Cw and Rw (root mean square), as derived in Appendix A. The calculated pecentage errors in Cw and Rw for the three different drag values are given in Table G3.

Table G3 Percentage errors

	percentage error	
Rt (N)	Cw	Rw
1,536	1,6	1,2
1,992	1,6	1,0
3,363	0,8	0,5

APPENDIX H

Derivation of the Model Shape Formula

The model hulls have waterlines which are arcs of circles, each waterline being defined by a different circle. The overall model length remains constant for all waterlines. Consider Figure H1.

Defining the following coordinate system with the origin at the lowest point on the hull, on the longitudinal axis of symmetry and on the flat side of the hull:

x = the transverse distance from the flat side towards the curved side

y = the longitudinal distance from the transverse axis of symmetry

z = the vertical distance from the lowest part of the hull

Also defining the following:

r(z) = the radius of each circle which defines the curved waterline profile

i(z) = the distance from the centre of the circle to the x coordinate

j(z) = the maximum hull thickness at each waterline

b = the model half length

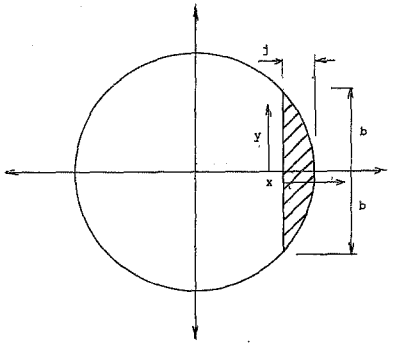

Figure B1 Circle and coordinates defining the model surface

For each circle we can write the following:

$$y^2+i^2 = r^2 \text{ (equation of a circle)} \qquad (H1)$$

$$2rj = j^2+b^2 \text{ (writing (H1) in terms of j and b)} \qquad (H2)$$

$$x = j-r+i \qquad (H3)$$

Solving the three equations simultaneously and eliminating r and p we get:

$$y^2 = (-x^2+j^2x-b^2x+jb^2)/j \qquad (H4)$$

The maximum hull thickness j at each waterline is a function of z and can be defined by a polynomial or exponential relationship. Figure H2 gives the coordinates, in millimetres, of the model midship section.

Thus any point on the hull surface can be defined mathematically in terms of x, y and z coordinates.

Formula for the Calculation of the Perimeter of a Waterline

For the purpose of calculating the model wetted surface area (see Appendix F), the perimeter of any given waterline is required. The perimeter, s is thus:

$$s = (\text{arc length of the defining circle})+2b$$

$$= 2r(\arcsin(b/r))+2b \qquad (H6)$$

Formula for the Calculation of the Area of a Waterline

This is required to calculate the model displacement (see Appendix F). By integrating (H1) between the limits (r-j) and r, the area, a of a waterline is:

$$a = 2((r^2\pi/4)-((r-j)\sqrt{(2rj-j^2)}/2) - (r^2(\arcsin((r-j)/r))/2)) \quad (H7)$$

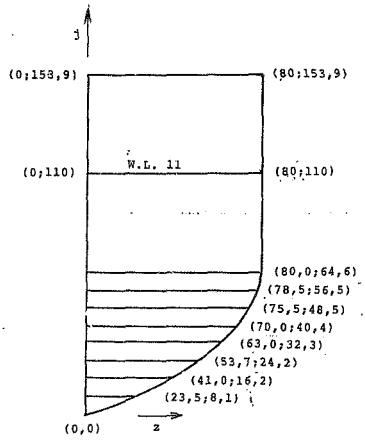

Figure H2 Coordinates, in millimetres, of the hull midship section

APPENDIX I

Effect of Size of Towing Tank on Model Resistance

The data which was used to calculate the expected increase in resistance due to the close proximity of the tank wall was taken from a publication by Comstock and Hancock[11], the curves in Figures I1, I2 and I3 being obtained through tests on a wide range of hull shapes.

A value for the "Displacement-Length Ratio" (as defined at the top of Figure I2) was calculated using the displacement of a single hull. A value of 217 was obtained for the model used in this project. The lowest curve in Figure I2 was used, this having the closest value of "Displacement-Length Ratio", i.e. 200.

Sample Calculations

The following is a sample calculation for the percentage error in resistance ratio due to to the model being in the proximity of the tank wall at a given speed and separation.

Model speed:

$$Fn = 0,33$$

This gives a value of 1,1 when converted to the scaling of $v/\sqrt{L}$ as defined in Figure I2. The intercept of this line with the Displacement-Length Ratio line gives a Y-intercept of 0,35. Thus:

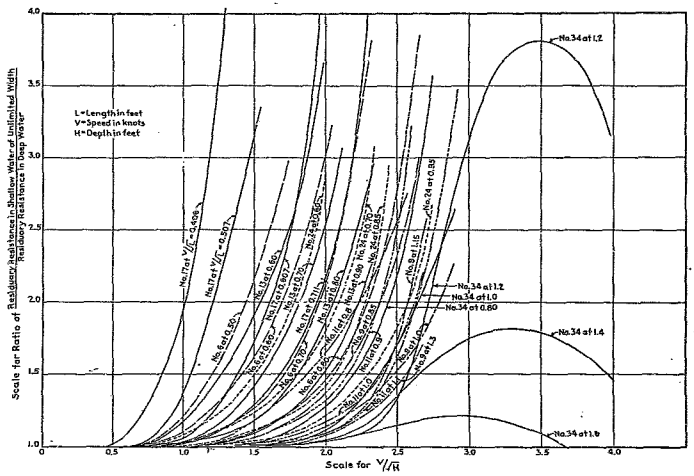

Figure 11 Approximate increase in resistance in shallow water of unlimited width, deduced from model tests (Comstock and Hancock[11])

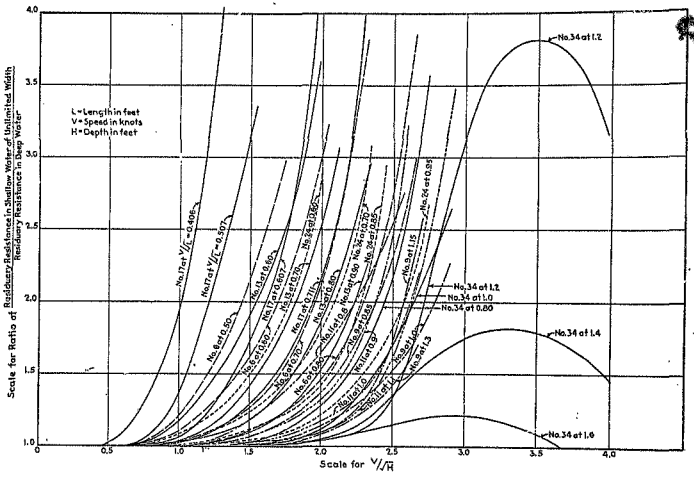

Figure 11 Approximate increase in resistance in shallow water of unlimited width, deduced from model tests (Comstock and Hancock[12])

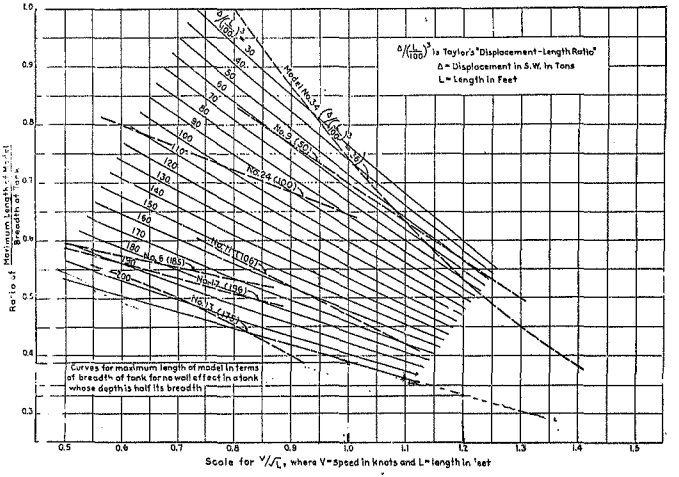

Figure 12 Maximum size of model for no measurable wall effect (Comstock and Hancock[11])

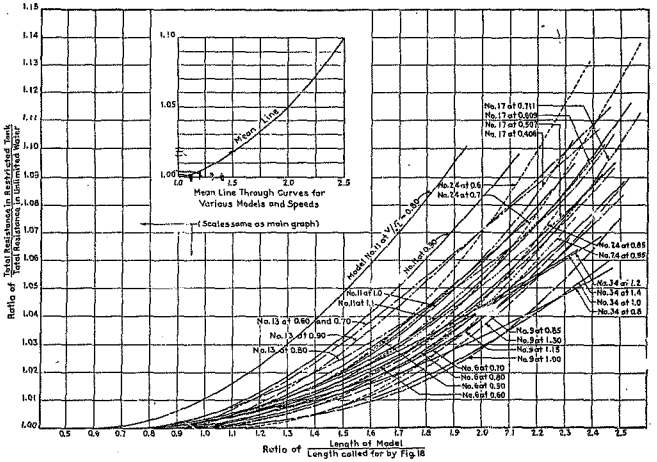

Figure 13 Increase in model resistance due to too large a model (Comstock and Hancock[11])

max. length of model/breadth of tank = 0,35

Hull separation:

S/L = 0,5

This puts the hull at a distance of 0,94 m from the tank wall, and hence an effective tank breadth of 1,88 m. Therefore:

max. length of model = 0,66 m

Referring now to Figure I3, the actual length of model was 0,8 m, and so the value for the X-intercept becomes:

0,8/0,66 = 1,22

This then gives a Y-intercept of 1,005, i.e. an increase in resistance of 0,5 per cent due to the proximity of the wall.

Because the resistance ratio Rw/Rwin is a comparison between the wave resistance at a given separation and speed with the wave resistance at infinite separation and at the same speed, the error due to wall proximity at infinite separation must also be calculated in the same way. At infinite separation the hull was 0,9 m from the tank wall, giving an effective tank breadth of 1,8 m. This also gives an increase in resistance of 0,5 per cent, implying an error in resistance ratio of zero per cent due to the proximity of the wall.

Author Dancig Anthony Aaron
Name of thesis Model Tests On Double-hull Wave Interference Effects Using A Gravity Dynamometer. 1987

PUBLISHER:
University of the Witwatersrand, Johannesburg
©2013

LEGAL NOTICES:

Copyright Notice: All materials on the University of the Witwatersrand, Johannesburg Library website are protected by South African copyright law and may not be distributed, transmitted, displayed, or otherwise published in any format, without the prior written permission of the copyright owner.

Disclaimer and Terms of Use: Provided that you maintain all copyright and other notices contained therein, you may download material (one machine readable copy and one print copy per page) for your personal and/or educational non-commercial use only.

The University of the Witwatersrand, Johannesburg, is not responsible for any errors or omissions and excludes any and all liability for any errors in or omissions from the information on the Library website.